RSC Advances

ROYAL SOCIETY OF CHEMISTRY

www.rsc.org/advances

Hetero Aromatic Donors as Effective Terminal Groups for DPP Based Organic Solar Cells

Marri Anil Reddy,[a] CH. Pavan Kumar,[a,b] Akudari Ashok,[a] Abhishek Sharma[c] G. D. Sharma[d]*, and Malapaka Chandrasekharam [a,b]*

[a]Network of Institutes for Solar Energy, CSIR-Indian Institute of Chemical Technology, I&PC Division, Uppal Road, Tarnaka, Hyderabad - 500 007, India.

[b]Academy of Scientific and Innovative Research, CSIR-IICT.

c Department of Electronics and Communication Engineering, LNMIIT, Jaipur, India.

[d]R & D Center for Science and Engineering, JEC Group of Colleges, Jaipur Engineering College Campus, Kukas, Jaipur 302028, India .

E-mail: chandra@iict.res.in phone Fax: +00914027193186 (M. Chandrasekharam).
gdsharma273@gmail.com and sharmagd_in@yahoo.com (G. D. Sharma).

Abstract

Four new solution-processable donor-acceptor-donor (D-A-D) structured low bandgap small molecules (**CSDPP5, CSDPP6, CSDPP7** and **CSDPP8)** with diketopyrrolopyrrole as central acceptor unit and phenoxazine (POZ) or carbazole (CBZ) as terminal units were designed, synthesized and characterized. The new small molecules have been employed as donors along with the $PC_{71}BM$ as electron acceptor in solution processed BHJ organic solar cells, showed broad absorption band with suitable electrochemical energy levels. When the BHJ active layer was cast from THF solvent, the optimal power conversion efficiencies obtained with **CSDPP5**, **CSDPP6**, **CSDPP7** and **CSDPP8** are 2.97% 3.06%, 2.42% and 2.43% respectively. The PCE of the devices when processed with DIO/THF solvent, have been further enhanced to 4.69%, 4.14% for **CSDPP6**:$PC_{71}BM$ and **CSDPP8:**$PC_{71}BM$ active layers respectively. The enhancement in PCE has been attributed to change in nanoscale morphology and more balanced charge transport resulting from increased hole mobility.

Key Words

Bulk hetero junction organic solar cells (BHJ OSCs), Thiophene functionalized DPP (TDPP), Solvent Additive, B3LYP/6-311 G(d,p) level theory.

1. Introduction

Recently, Organic solar cells (OSCs) have been evolving into promising clean and renewable energy sources, owing to their low-cost, flexibility and applicability in large area device. [1-6] In general, OSCs feature a bulk hetero junction (BHJ) structure, where conjugated polymers and a fullerene derivative serve as the electron donor (D) and acceptors (A) respectively. Significant recent advancements in the power conversion efficiency (PCE) of OSCs have been reported and a PCE of over 10% have been achieved through careful material design and device optimization[7-14] for single junction while for a tandem junction OSCs over 11% have been achieved.[15,16] However, conjugated polymers suffer from batch to batch variation in terms of molecular weight and polydispersity that affect the processability and thus semiconducting properties.[16-18] BHJ solar cells based on solution processed small molecule have been recently investigated[19-23] and achieved a PCE of 8% for single junction solar cells[24-26] and 10.1% for tandem solar cells[27]. Recently, Chen et al have achieved a record PCE of about 10 % for single junction solution processed small molecule organic solar cell[28] which is very close to the best polymer organic solar cells. To date an impressive PCE of 12% has been achieved for a vacuum processed triple junction tandem solar cell based on small molecules.[29]

Among the various donor building blocks investigated, diketopyrrolopyrrole (DPP), based molecules are promising candidates due to the favorable properties of the DPP unit, e.g., strong light absorption, photochemical stability, excellent charge carrier mobility, and easy synthesis. [30-39]Alkyl Substitution on the nitrogen atoms in the DPP unit can improve the solubility of the DPP molecules. Thiophene functionalized DPPs (TDPP) have attracted extensive applications in organic optoelectronics. This is due to the fact that the electron richness of the thiophene moiety can induce strong intramolecular charge transfer with the electron deficient DPP core and π-π stacking of conjugating units improves the optical and electrochemical properties. The highly efficient solution processed small molecule donor materials based on DPP can be classified into two categories according to their D/A structures, i.e. either DPP as the electron acceptor unit capped with two donor units (D-A-D), or donor unit end capped with two DPP as the acceptor. The overall PCEs of DPP donor molecules reported so far in literature is less than 5%. However, the extension of conjugated backbone to DPP-containing polymers achieved the PCE of about 6.5 %.[40-42] More recently, the highest efficiency of about 7 % has been reported for OSCs using solution processed DPP based small molecules.[43] Thus DPP based materials functionalized with D-A structures will

have potential in high performance solar cells. In this context, phenoxazine (POZ) is known to be a good conjugated heterocyclic compound with electron rich oxygen and nitrogen heteroatoms. Recently, Sun et al synthesized A-π-D-π-A small molecule employing POZ as core unit and dicyanovinyl as electron withdrawing end group for BHJ solar cell and achieved a PCE of about 5.6 %.[44]

In this line of work, our group demonstrated the use of thiophene diketopyrrolopyrrole (TDPP) based molecular semiconductors as donor materials in BHJ solar cells and achieved moderate PCE. [45,46] Recently, we have reported four new simple D–A–D structured DPP molecules (**CSDPP9-CSDPP12**) with DPP as central core unit and different electron donating groups as terminal units. The BHJ devices, based on **CSDPP11**:$PC_{71}BM$ and **CSDPP12**:$PC_{71}BM$ subjected to solvent and thermal annealing showed PCEs of 5.47% and 4.88% respectively.[47] To further examine the effect of hetero aromatic donor units on the properties of TDPP based molecules, we have successfully synthesized four D-A-D structured small molecules, all of which contain thiophene capped DPP, i.e. with ethyl-hexyl (**CSDPP6** and **CSDPP8**) and n-decyl long chain (**CSDPP5** and **CSDPP7**) as acceptor core and different donor carbazole (CBZ) **CSDPP7** and **CSDPP8** and phenoxazine (POZ) **CSDPP5** and **CSDPP6** (figure 1) as arms. These small molecule donors exhibit excellent solubility in common organic solvents. In addition, their photophysical and electrochemical properties show that they harvest sunlight across the visible spectrum range and have appropriate HOMO and LUMO energy levels to satisfy the requirement of donor component for solution processed BHJ OSCs. Therefore, we have explored the photovoltaic properties of these new donors in BHJ solar cells with the structure ITO/PEDOT:PSS/donors:$PC_{71}BM$/Al. The PCE for the devices from **CSDPP5**, **CSDPP6, CSDPP7** and **CSDPP8** as donor approached 2.97 %, 3.06 %, 2.42 % and 2.43 %, respectively and further improved up to 4.69 % and 4.14 % for the device using **CSDPP6**:$PC_{71}BM$ and **CSDPP8**:$PC_{71}BM$ active layers, respectively, processed with (1,8-diiodooctane) DIO/THF solvent.

2. Experimental details

2.1 Materials and instrumentation

The starting materials and reagents, carbazole, phenoxazine, thiophene carbonitrile, di-n-ethylsuccinate, *tert*-BuOK, *tert*.amyl alcohol, bromodecane, 2-ethyl hexyl bromide, bis(pinacalato)diboron and *N*-bromosuccinimide were purchased from Sigma-Aldrich. The solvents were purified by standard procedures and purged with nitrogen before use. All other

chemicals used in this work were analytical grade and were used without further purification, and all reactions were performed under argon atmosphere unless and otherwise mentioned. Chromatographic separations were carried out on silica gel (60–120 mesh). ^{1}HNMR spectra were recorded on Bruker 300 MHz spectrometer using TMS as an internal standard. Mass spectra were recorded on Shimadzu LCMS- 2010 EV model with ESI probe. Absorption spectra were recorded on a Shimadzu UV-Vis to near IR region 3600 spectrometer. Electrochemical data were obtained by cyclic voltammetry using a conventional three-electrode cell and a BAS100 electrochemical analyzer. C, H, N, S data was recorded on Elementar (variomicrotube) instrument.

2.2 Synthesis of 10-hexyl-10H-phenoxazine (1)

To an ice-cooled suspension of NaH (0.314 g, 13.099 mmol) in DMF (30 mL) was added phenoxazine (2.00 g, 10.916 mmol) and stirred for 30 min at room temperature. Hexyl bromide (1.964 mL, 13.099 mmol) was added drop wise to the reaction mixture and then stirred for 16 h under N_2. After removing the solvent, the resulting mixture was washed with ice water and extracted with EtOAC and dried over Na_2SO_4. After evaporation, the crude compound obtained was purified by silica gel column chromatography. The desired compound was eluted using *n*-hexane/ethylacetate (9/1; v/v) to give viscous liquid **1** (82%). ^{1}H NMR (300 MHz, $CDCl_3$, δ): 6.68-6.73 (m, 2H), 6.56 (d, 4H), 6.38 (d, 2H), 3.44 (t, 2H), 1.60-1.70 (m, 2H), 1.34-1.43 (m, 6H), 092 (t, 3H). ^{13}C NMR (75 MHz, $CDCl_3$, δ): 144.97, 133.37, 123.51, 120.57, 115.23, 111.19, 44.05, 31.53, 26.55, 24.84, 22.62, 13.97. ESI-MS**:** m/z $[M]^+$: 268.

2.3 Synthesis of 3-bromo-10-hexyl-10H-phenoxazine (2)

To a solution of compound **1** (0.700 g, 2.621 mmol) in anhydrous chloroform (40 mL) was added *N*-bromosuccinimide (0.560 g, 3.146 mmol) portion wise in an ice-water bath. After complete addition, the solution mixture was warmed to room temperature and stirred for 6 h. The resulting solution was washed with water and brine. The organic phase was dried over Na_2SO_4 and the solvent was removed. The residue was purified by silica gel chromatography using ethyl acetate:hexane (1:9) as eluent to afford viscous liquid **2** (75%). ^{1}H NMR (300 MHz, $CDCl_3$, δ): 6.84-6.89 (m, 1H), 6.76-6.82 (m, 1H), 6.71-6.73 (m, 1H), 6.58-6.66 (m, 2H), 6.45 (d, 1H), 6.28 (d, 1H), 3.35-3.48 (brs, 2H), 1.56-1.69 (m, 2H), 1.33-1.43 (m, 6H), 0.91 (t, 3H). ^{13}C NMR (75 MHz, $CDCl_3$, δ): 145.65, 144.50, 132.77, 126.48, 126.08, 123.92, 120.90, 118.50, 118.31, 115.42, 112.15, 111.36, 44.13, 31.52, 26.52, 24.71, 22.63, 13.99. ESI-MS: m/z $[M+2H]^+$: 348.

2.4 Synthesis of 10-hexyl-3-(4, 4, 5, 5-tetramethyl-1,3,2-dioxaborolan-2-yl)-10H-phenoxazine (3)

A solution of compound **2** (0.500 g, 1.272 mmol), bis(pinacolato)diboron (0.388 g, 1.399 mmol), KOAc (0.374 g, 3.817 mmol), and Pd(dppf)Cl_2 (0.056 g, 0.076 mmol) in dry dimethoxy ethane (8 mL) was refluxed at 85 ^{0}C under a nitrogen atmosphere for 16 h. After being cooled to room temperature, the mixture was poured into water (20 mL) and the organic layer was separated. The aqueous layer was extracted with dichloromethane (3×20 mL) and the combined organic layers were dried over anhydrous Na_2SO_4. The solvent was evaporated under reduced pressure and the crude product was pre-adsorbed onto silica gel and chromatographed (8:2 *n*-hexane/ethyl acetate) to give viscous liquid **3** (75%). ^{1}H NMR (300 MHz, $CDCl_3$, δ): 7.23-7.25 (m, 1H), 7.02 (s, 1H), 6.77 (t, 1H), 6.57-6.64 (m, 2H), 6.42-6.51 (m, 2H), 3.35-3.58 (brs, 2H), 1.64 (q, 2H), 1.34-1.42 (m, 6H), 1.31 (s, 12H), 0.91 (t, 3H). ^{13}C NMR (75 MHz, $CDCl_3$, δ): 145.20, 144.20, 134.66, 131.02, 127.64, 123.35, 121.10, 120.83, 115.32, 111.39, 110.56, 83.44, 43.93, 31.50, 26.49, 24.77, 22.59, 13.99. ESI-MS: m/z $[M+H]^+$: 394

2.5 Synthesis of 9-hexyl-9H-carbazole (4)

Compound **4** was synthesized according to the procedure as described above for synthesis of **1**. Nature: white solid Yield: 90%. ^{1}H NMR (300 MHz, $CDCl_3$, δ): 8.03 (d, 2H), 7.32-7.41 (m, 4H), 7.16 (t, 2H), 4.28 (t, 2H), 1.86 (q, 2H), 1.26-1.41 (m, 6H), 0.86 (t, 3H). ^{13}C NMR (75 MHz, $CDCl_3$, δ): 140.345, 125.497, 122.733, 120.274, 118.618, 108.594, 42.986, 31.553, 28.883, 26.934, 22.522, 14.003. ESI-MS: m/z $[M+H]^+$: 252.

2.6 Synthesis of 3-bromo-9-hexyl-9H-carbazole (5)

Compound **5** was synthesized according to the procedure as described above for synthesis of **2**. Nature: light yellow color solid Yield: 75%. ^{1}H NMR (300 MHz, $CDCl_3$, δ): 8.18 (s, 1H), 8.02 (d, 1H), 7.44-7.53 (m, 2H), 7.37 (d, 1H), 7.19-7.26 (m, 2H), 4.23 (t, 2H), 1.82 (q, 2H), 1.25-1.36 (m, 6H), 0.84 (t, 3H). ^{13}C NMR (75 MHz, $CDCl_3$, δ): 140.573, 138.921, 128.857, 128.086, 126.225, 124.421, 122.937, 121.680, 120.428, 119.068, 110.014, 108.835, 43.057, 31.480, 28.790, 26.854, 22.484, 13.977. ESI-MS: m/z $[M+H]^+$: 330.

2.7 Synthesis of 9-hexyl-3-(4,4,5,5-tetramethyl-1,3,2-dioxaborolan-2-yl)-9H-carbazole (6)

Compound **6** was synthesized according to the procedure as described above for synthesis of **3.** Nature: yellow color solid Yield: 73%. ^{1}H NMR (300 MHz, $CDCl_3$, δ): 8.59 (s, 1H), 8.12 (d, 1H), 7.91 (d, 1H), 7.45 (t, 1H), 7.37-7.40 (m, 2H), 7.23 (t, 1H), 4.29 (t, 2H), 1.86 (q, 2H), 1.39 (s, 12H), 1.25-1.33 (m, 6H), 0.85 (t, 3H). ^{13}C NMR (75 MHz, $CDCl_3$, δ): 142.549,

140.456, 132.038, 127.699, 125.519, 123.063, 122.540, 120.475, 119.119, 108.653, 108.011, 83.479, 43.008, 31.503, 28.828, 26.862, 24.886, 22.459, 13.938. ESI-MS: m/z $[M+H]^+$: 378.

2.8 Synthesis of 3,6-Dithiophen-2-yl-2,5-dihydro-pyrrolo[3,4-c]pyrrole-1,4-dione (7)

3,6-Dithiophen-2-yl-2,5-dihydro-pyrrolo[3,4-c]pyrrole-1,4-dione was synthesized according to a reported procedure.[48-50]

2.9 Synthesis of 2,5-Di-*n*-decyl-3,6-dithiophen-2-yl-pyrrolo[3,4-c]pyrrole-1,4-dione (8)

Compound **8** was synthesized according to a reported procedure to give purple brown shiny crystalline powder (Yield: 75.4%).[18]

2.10 Synthesis of 2,5-bis(2-ethylhexyl)-3,6-dithiophen-2-yl-pyrrolo[3,4-c]pyrrole-1,4-dione (9)

In a three-necked, oven-dried 250 mL round-bottom flask, compound **7** (3.00 g, 10.0 mmol) and anhydrous K_2CO_3 (4.15 g, 30.0 mmol) in 100 mL of anhydrous DMF were heated to 120 °C under N_2 for 1 h. 2-ethylhexyl bromide (4.80 mL, 25.0 mmol) was then added dropwise, and the reaction mixture was further stirred overnight at 130 °C. After cooling to room temperature, 400 mL of distilled water was added and stirred for 1 h, the mixture was filtered. The solid obtained was washed with several portions of distilled water, methanol, and then air-dried. The crude product was purified by flash chromatography using chloroform as eluent, and the solvent was removed in vacuum to obtain a brown color solid (Yield: 75%). ^{1}H NMR (300 MHz, $CDCl_3$, δ): 8.90 (d, 2H), 7.64 (d, 2H), 7.29 (t, 2H), 3.98-4.08 (m, 4H), 1.88-1.83 (m, 2H), 1.40-1.20 (m, 16H), 0.90 (m, 12H).

2.11 Synthesis of 3,6-Bis-(5-bromo-thiophen-2-yl)-2,5-di-decyl-pyrrolo[3,4-c]-pyrrole-1,4-dione (10)

The compound **10** was synthesized according to the reported procedure to give dark purple brown powder (Yield: 64%).[18]

2.12 Synthesis of 3,6-Bis-(5-bromo-thiophen-2-yl)-2,5-bis(2-ethylhexyl)-pyrrolo[3,4-c]-pyrrole-1,4-dione (11)

In a three-necked, oven-dried, 150 mL round-bottom flask, compound **9** (1 g, 1.908 mmol) was dissolved in 40 mL of anhydrous $CHCl_3$, covered with aluminum foil, and stirred at room temperature under N_2 for 15 min. *N*-bromosuccinimide (0.781 g, 4.389 mmol) was then added, and the reaction mixture was stirred at room temperature for 12 h. The mixture was then poured into 100 mL of methanol, and the resulting suspension was further stirred at room temperature for 1 h. The solid precipitated was collected by vacuum filtration and washed with several portions of hot distilled water and hot methanol to obtain brown color

solid (65%). ^{1}H NMR (300 MHz, $CDCl_3$, δ): 8.84 (d, 2H), 7.62 (d, 2H), 3.98-4.08 (m, 4H), 1.90-1.80 (m, 2H), 1.40-1.20 (m, 16H), 0.90 (m, 12H). ESI-MS: m/z $(M+4H)^+$: 685.

General procedure for the synthesis of CSDPP5 and CSDPP7

A 50 mL of Schlenk tube was charged with compound **3** or **6** (0.679 mmol), $Pd(PPh_3)_4$ (0.062 g, 0.054 mmol). Dimethoxy ethane (8 mL) and 2M aqueous sodium carbonate (2 mL) were added, and the tube was purged with argon gas with 5 evacuate/refill cycles. Compound **10** (0.200 g, 0.271 mmol) was subsequently added as a neat liquid. The tube was sealed and heated at 90 °C vigorously for 18 h. Upon cooling to ambient temperature, the organics were extracted into dichloromethane (3×30 mL) from 30 mL water. The combined organics were washed with water (1×30 mL) and brine (1×30 mL), dried over Na_2SO_4, filtered and the solvent was removed under reduced pressure to give **CSDPP5 and CSDPP7.**

2.13 2,5-didecyl-3,6-bis(5-(10-hexyl-10H-phenoxazin-3-yl)thiophen-2-yl)pyrrolo[3,4-c]pyrrole-1,4(2H,5H)-dione (CSDPP5) (dark blue solid, 46%). ^{1}H NMR (300 MHz, $CDCl_3$, δ): 8.88-9.02(brs, 2H), 7.20-7.35(m, 4H), 6.96-7.10(m, 2H), 6.75-6.80(m, 4H), 6.61-6.68(m, 4H), 6.34-6.43(m, 4H), 4.05(t, J=7.74 Hz, 4H), 3.33-3.47(brs, 4H), 1.75(br, 4H), 1.57-1.68(m, 6H), 1.25-1.37(m, 38H), 0.84-0.94(m, 12H). FT-IR (KBr), cm^{-1}: 3059, 2921, 2850, 1654, 1592, 1551, 1491, 1430, 1380, 1271, 1072, 1024, 908, 854, 789, 728. Anal. Cal.: $C_{70}H_{86}N_4O_4S_2$. C: 75.64, H: 7.80, N: 5.04, S: 5.77 Found- C: 75.32, H: 7.82, N:5.03, S: 5.73.

2.14 2,5-didecyl-3,6-bis(5-(9-hexyl-9H-carbazol-3-yl)thiophen-2-yl)pyrrolo[3,4-c]pyrrole-1,4(2H,5H)-dione (dark blue solid, CSDPP7) (58%). ^{1}H NMR (300 MHz, $CDCl_3$, δ): 9.02 (d, J=4.20 Hz, 2H), 8.36 (s, 2H), 8.16 (d, J=7.80 Hz, 2H), 7.77 (d, J=6.90 Hz, 2H), 7.48-7.53 (m, 4H), 7.38-7.41 (m, 4H), 7.29 (d, J=7.20 Hz, 2H), 4.28 (t, J=7.80 Hz, 4H), 4.16 (t, J=7.50 Hz, 4H), 1.78-1.92 (m, 8H), 1.25-1.53 (m, 40H), 0.82-0.89 (m, 12H). FT-IR (KBr), cm^{-1}: 3051, 2919, 2850, 1650, 1597, 1544, 1467, 1428, 1336, 1273, 1216, 1186, 1147, 1071, 1018, 958, 860, 787, 725, 622, 489. Anal. Cal.: $C_{70}H_{86}N_4O_2S_2$. C: 77.88, H: 8.03, N: 5.19, S: 5.94 Found- C: 77.84, H: 8.02, N: 5.17, S: 5.92.

General procedure for the synthesis of CSDPP6 and CSDPP8.

The synthetic procedure followed for **CSDPP6** or **CSDPP8** is similar to the preparation of the compounds **CSDPP5** or **CSDPP7** employing compound **11** (0.200 g, 0.293 mmol) in place of compound **10**. The products were purified by column chromatography on silica (4:6 dichloromethane/hexane) to afford either **CSDPP6 or CSDPP8.**

2.15 2,5-bis(2-ethylhexyl)-3,6-bis(5-(10-hexyl-10H-phenoxazin-3-yl)thiophen-2-yl)pyrrolo[3,4-c]pyrrole-1,4(2H,5H)-dione (CSDPP6) (dark blue solid, 48%). ^{1}H NMR

(300 MHz, $CDCl_3$, δ): 8.93-9.00 (brs, 2H), 7.27-7.29 (m, 2H), 7.08-7.10 (d, J=8.10 Hz, 2H), 6.88 (s, 2H), 6.77-6.83 (m, 2H), 6.63-6.70 (m, 4H), 6.42-6.49 (m, 4H), 4.04 (d, J=7.20 Hz, 4H), 3.42-3.52 (brs, 4H), 1.90-1.99 (m, 2H), 1.66 (q, J=6.60 Hz, J=14.70 Hz, 4H), 1.24-1.42 (m, 28H), 0.86-0.97 (m, 18H). FT-IR (KBr), cm^{-1}: 3076, 2955, 2924, 2854, 1653, 1589, 1552, 1489, 1420, 1382, 1277, 1227, 1156, 1072, 1025, 863, 834, 794, 734. Anal. Cal.: $C_{66}H_{78}N_4O_4S_2$. C: 75.10, H: 7.45, N: 5.31, S: 6.08 Found- C: 75.12, H: 7.41, N:5.29, S: 6.02.

2.16 2,5-bis(2-ethylhexyl)-3,6-bis(5-(9-hexyl-9H-carbazol-3-yl)thiophen-2-yl)pyrrolo[3,4-c]pyrrole-1,4(2H,5H)-dione (dark blue solid, CSDPP8) (56%). ^1H NMR (300 MHz, $CDCl_3$, δ): 9.03 (d, J=4.80 Hz, 2H), 8.36 (s, 2H), 8.15 (d, J=8.40 Hz, 2H), 7.77 (d, J=6.90 Hz, 2H), 7.47-7.53 (m, 4H), 7.39-7.42 (m, 4H), 7.29 (d, J=7.50 Hz, 2H), 4.28 (t, J=6.60 Hz, 4H), 4.12 (dd, J=3.90 Hz, J=3.60 Hz, 4H), 1.99-2.03 (m, 2H), 1.87 (q, J=7.80 Hz, J=8.10 Hz, 4H), 1.25-1.46 (m, 28H), 0.84-0.97 (m, 18H). FT-IR (KBr), cm^{-1}: 3057, 2923, 2854, 1654, 1596, 1548, 1485, 1427, 1328, 1265, 1229, 1149, 1077, 1022, 873, 794, 732, 623, 418. Anal. Cal.: $C_{66}H_{78}N_4O_2S_2$. C: 77.45, H: 7.65, N: 5.47, S: 6.27 Found- C: 77.43, H: 7.62, N:5.45, S: 6.25.

2.17 Device fabrication and characterizations

The BHJ OSCs were prepared using the indium tin oxide (ITO) coated glass substrate as anode, Al as cathode and a blended film of **CSDPP5** or **CSDPP6 or CSDPP7 or CSDPP8 (CSDPP**:$PC_{71}BM$) as photoactive layer as follows: Firstly, ITO coated glass substrates were cleaned with detergent, ultrasonicated in acetone and isopropyl alcohol, and subsequently dried in an oven for 12 h. An aqueous solution of PEDOT:PSS (Heraeus, Clevious P VP, Al 4083) was spin cast on the ITO substrates obtaining a film of about 40 nm thick. The PEDOT:PSS film was then dried for 10 min at a temperature of 120° C in ambient conditions. Then, a 15 mg/mL solution of **CSDPP**/$PC_{71}BM$ blends in different solvents were prepared with different weight ratio and then spun cast on the top of PEDOT:PSS layer and then dried at 80° C for 10 min. THF and DIO/THF (1, 2, 3 and 4 % (v %) of DIO) were used as solvents for spun cost. The thickness of the photoactive layer is about 100 ± 10 nm. Finally ~ 90 nm thick Al electrode was deposited on the top of BHJ film under reduced pressure

($<10^{-6}$ Torr). All the devices were fabricated and tested in ambient atmosphere without encapsulation. The active area of the devices is about 20 mm^2.

The current–voltage characteristics of the devices were measured using a computer controlled Keithley 238 source meter in dark as well as under illumination intensity of 100 mW/cm^2. A xenon light source coupled with AM1.5 optical filter was used as light source. The incident photon to current efficiency (IPCE) of the devices was measured illuminating the device through the light source and monochromator and resulting current was measured using Keithley electrometer under short circuit condition.

2.18 Computational Details

All the calculations have been performed using the Gaussian 09 program package.[51] Geometrical optimization was performed in vacuo using B3LYP[52,53] exchange-correlation functional and a 6-311G(d, p) basis set.[54] The optimized geometries were then used to obtain frontier molecular orbitals (FMOs). To simulate the optical spectra, the lowest spin allowed singlet–singlet transitions were computed on the ground state geometry. TDDFT calculations of the lowest singlet–singlet excitations were performed in THF solution, on the optimized geometries using the B3LYP/6-311G (d, p) level of theory. The integral equation formalism polarizable continuum model (PCM)[55] within self-consistent reaction field (SCRF) theory, has been used to describe the solvation of the molecules. The software GaussSum 2.2.5[56] was utilized to simulate the major portion of absorption spectrum and to analyze the nature of transitions. The percentage contributions of individual moieties of the dyes to the respective molecular orbitals have also been calculated.

3. Results and discussion

3.1 Synthesis of CSDPP 5-CSDPP8:

The synthetic route to **CSDPP5-CSDPP8** sensitizers were depicted in scheme 1. The commercially available starting materials phenoxazine and carbazole were N-alkylated using NaH as base in DMF followed by bromination in presence of *N*-bromosuccinimide. The Miyaura borylation of the bromo substituted compounds **2** and **4** with bis(pinacolato)-diborane (B_2Pin_2) under $PdCl_2$(dppf) catalysed reaction in presence of KOAc and 1,2-dimethoxyethane, resulted in compounds **3** and **6**. The DPP derivative **7** was synthesized according to a reported procedure,[49-51] followed by N-alkylation with 1-bromodecane and 2-ethylhexylbromide to afford pure N-alkylated products **8** and **9**. Compounds **8** and **9** were

further subjected to bromination with NBS to afforded dibromo compounds **10** and **11**. The target sensitizers **CSDPP5-CSDPP8** were prepared employing the $Pd(PPh_3)_4$ assisted Suzuki coupling reaction of **3** or **6** with compound **10** and **11** in yields of 46-58% respectively.

3.2 Optical and electrochemical properties

The UV-Visible absorption spectra of the DPP small molecules (**CSDPP5-CSPP8**) in THF solution and in film (THF solution) are shown in figure 2(a) and 2(b) respectively and the corresponding maximum absorption wavelengths (λ_{max}) are compiled in table 1. The λ_{max} of **CSDPP5** and **CSDPP6** solution was observed at 647 nm (Molar extinction coeff. (ε), 6.3899 M^{-1} cm^{-1} and 6.5494 M^{-1} cm^{-1}), while λ_{max} for **CSDPP7** and **CSDPP8** was observed at 623 nm (ε, 6. 9098 M^{-1} cm^{-1} and 6.5046 M^{-1} cm^{-1}), resulting from the intramolecular charge transfer (ICT) transition between the donor and acceptor units in the conjugated small molecules. The small molecules **CSDPP5** and **CSDPP6** exhibited red shift in the absorption band compared to **CSDPP7** and **CSDPP8** indicating an enhanced ICT transition band which is resulting from the better donating capacity of Phenoxazine. The thin films of these small molecules exhibited similar absorption trend with broader and red shifted which is attributed to π-π intermolecular interactions in the solid state. The optical bandgap for these small molecules was estimated from the onset absorption wavelength in thin film and are 1.65 eV, 1.66 eV, 1.77 eV, and 1.78 eV for **CSDPP5**, **CSDPP6, CSDPP7** and **CSDPP8**, respectively. The lower value of optical bandgap for **CSDPP5** and **CSDPP6** reflects a higher amount of charge transfer between the DPP acceptor core and conjugated arms for phenoxazine donor as compared to carbazole. It is well known that the broader absorption and lower bandgap are beneficial to improve the light harvesting efficiency of the active layer, resulting higher photocurrent generation. We expect higher photocurrent for **CSDPP5** and **CSDPP6** as compared to **CSDPP7** and **CSDPP8**.

In order to provide in-depth insight into the electronic structures of **CSDPPs**, theoretical calculations based on the DFT method at the B3LYP/6-311G(d,p) level were carried out, in which the N-hexyl group was replaced by N-methyl for simplicity. The optimized geometries of **CSDPP5-CSDPP8** at B3LYP/6-311 G(d,p) level theory are shown in figure S1.The TDDFT studies of these molecules in THF are in nearly good agreement with experimental UV-Vis spectra. The spectra have been produced by convoluting Gaussian functions with FWHM = 0.30 eV. The normalized plots of simulated and experimental UV-Vis spectra of **CSDPPs** are depicted in figure 3. The respective summarized data of important allowed transitions is reported in ESI†. The wavelength of the excitations with the largest

oscillator strengths (f) within these bands are given in table 2. The most intense singlet transition is a HOMO to LUMO transition at 615 nm (f = 1.2162) for **CSDPP5**, 624 nm (f = 1.2145) for **CSDPP6**, 606 nm (f = 1.5051) for **CSDPP7** and 615 nm (f = 1.4894) for **CSDPP8**. The optimized geometry parameters, and detailed list of the calculated energy levels at the B3LYP/6-311G(d,p) level of theory are shown in ESI.†.

The highest occupied molecular orbital (HOMO) energy levels of these small molecules in thin films have been determined from the cyclic voltammetry (CV) (figure 4a) and compiled in table 1. The CV of these compounds exhibited a reversible oxidation wave where the HOMO level of these compounds were estimated from the onset oxidation potential under the assumption that energy level of Fc/Fc^{+} was 4.7 eV below the vacuum level. The lowest unoccupied molecular orbital (LUMO) energy level of these small molecules was estimated from the difference of HOMO energy level and $E_{0\text{-}0}$, where $E_{0\text{-}0}$ derived from the intersection of the absorption and emission spectra and compiled in table 1. It can be seen from the table 1 that the deeper HOMO energy level for **CSDPP5** (-5.24 eV) (**CSDPP6** (-5.23 eV) **CSDPP7** (-5.30 eV) and **CSDPP8** (-5.32 eV) is beneficial for high V_{oc}. The difference in HOMO energy level of **CSDPP5**, **CSDPP6** and **CSDPP7, CSDPP8** are attributed to the different donor units, i.e. POZ and CBZ respectively, while the LUMO energy level of four DPPs is almost same. The HOMO level of **CSDPP5** is identical to that of **CSDPP6** and **CSDPP7** showed almost similar to **CSDPP8**. The deeper lying HOMO levels and sufficient LUMO offsets (>0.6 V), (figure 4b) allow these small molecules to serve as electron donors in combination with $PC_{71}BM$ as an acceptor, which has HOMO and LUMO levels of -6.1 eV and -4.1 eV, respectively.

To understand the nature of charge transfer in the electronic transitions, we have plotted the isodensity surface plots (isovalue = 0.02) of the HOMO, LUMO and important nearest molecular orbitals (figure S2) which are involved in transitions with strong contributions to the first excitation as well as to next two excitations with strong oscillator strength. To gain further insight into the electron density distribution in each molecule, partial electron density contribution and terminal moieties in each molecule from the respective frontier orbitals have been generated and depicted in figure S3. For all the **CSDPPs** the HOMO and LUMO extend at least over all of their main inner body up to thiophene moieties. The HOMO-2 is majorly localized over the terminating groups while LUMO+2 localized at various degrees over the whole of the structure. We partition the structures into the diketopyrrolopyrrole (DKPP), the thiophene moieties (Th), and terminal groups Phenothiazine (PTZ), carbazole (CBZ) for **CSDPP5**, **CSDPP6**, **CSDPP7** and **CSDPP8**

respectively. The HOMO of **CSDPPs** has contributions from DKPP by (42%, 43%, 48% and 47%), Th (25%, 26%, 30%, 30%) and the terminal groups (33%, 32%, 23%, 22%) respectively. The LUMO of **CSDPPs** is dominated by contributions from the DKPP and Th groups by 52%, 52%, 54%, 54% and 37%, 37%, 37%, 37% respectively, with only minor contribution 11%, 11%, 9%, and 9% from the PTZ and CBZ moieties, respectively.

The calculated HOMO, LUMO energies and the HOMO-LUMO gap (HLG) at a B3LYP/6-311g(d,p) level in THF solvent is given in figure 5. The HOMO-LUMO gaps are shown in table 2.

The dipole moment of the organic molecules depends on the charge transfer process within the molecule, which in turn depends on the availability of electron donating group.[57] From table 2, PTZ (electron donor) containing CSDPPs showed higher dipole moment compared to CBZ containing molecules, due to higher electron donating capacity of PTZ moiety. The higher dipole moment of CSDPP6 might be attributed to more electrons donating nature and structural arrangement of 2-ethylhexyl moiety on nitrogen.

3.3 Photovoltaic properties

In BHJ OSCs, the relative quantities of donor and acceptor materials employed in the active layer is of great importance for the photovoltaic performance, since there should be a balance between the absorbance and charge transporting network of the active layer. When the acceptor content is low, the electron transporting ability will be limited, while when the acceptor content is too high, the absorbance and hole transporting ability of the active layer will be decreased. In the present investigation, $PC_{71}BM$ has been employed as acceptor, since it possesses high absorption in the visible region as compared to $PC_{61}BM$. BHJ active layers with a mixture of DPPs and $PC_{71}BM$ in THF in different weight ratios were tested and optimum ratio is 1:2. We are discussing our results with the optimum blend ratio. The optical absorption spectra of the blends were shown in figure 6 (for **CSDPP5**:$PC_{71}BM$ and **CSDPP7**:$PC_{71}BM$ blend films showed similar absorption profile to **CSDPP6**:PC71BM and **CSDPP8**:$PC_{71}BM$ blends, respectively), showed broad absorption covering from 350 to 700 nm with two absorption bands, corresponding to the $PC_{71}BM$ (shorter wavelength region) and DPPs (longer wavelength region), indicating that both donor and acceptor are contributing to the exciton generation and thereby photocurrent generation.

Solution processed BHJ solar cells based on these DPP small molecules were fabricated with a conventional structure glass/ITO/PEDOT:PSS/active layer/Al and the J-V characteristics of the devices are shown in figure 7a (**CSDPP5** and **CSDPP7**) and figure 8a (**CSDPP6** and **CSDPP8**), under illumination at AG1.5 G, 100 mW/cm^2 and the photovoltaic

parameters are summarized in table 3. With optimized weight ratio (1:2), the device based on **CSDPP5**:$PC_{71}BM$ and **CSDPP6**:$PC_{71}BM$ (cast with THF solvent) showed a PCE of 2.97 % (Jsc= 7.88 mA/cm^2, V_{oc}=0.84 V and FF= 0.47) and 3.06 % (J_{sc} of 7.92 mA/cm^2, V_{oc} of 0.84V and FF of 0.46), respectively. In contrast device fabricated with **CSDPP7**:$PC_{71}BM$, **CSDPP8**:$PC_{71}BM$ processed under same conditions produced lower PCE of 2.42 % (6.34 mA/cm^2, V_{oc} =0.91 V and FF=0.42) and 2.43 % (J_{sc} of 6.42 mA/cm^2, V_{oc} of 0.90 V and FF of 0.42), respectively. **CSDPP5** and **CSDPP7** have DPP core with n-decyl long side chain, whereas **CSDPP6** and **CSDPP8** have same DPP core with ethyl-hexyl side chain indicates that the alkyl modification in the DPP core does not have much influence in the solar cells performance. The difference in the photovoltaic performance is mainly due to the different end capping donor unit. Therefore we are discussing the detailed analysis of **CSDPP6** and **CSDPP8** based devices. The higher value of V_{oc} for **CSDPP8** based device as compared to the **CSDPP6** counter part is attributed to its deeper HOMO level than **CSDPP6**. However, the larger value of PCE of **CSDPP6** based device as compared to **CSDPP8** is due the higher values of J_{sc} and FF. The enhancement in J_{sc} is mainly due to the better light harvesting property of **CSDPP6** as compared to **CSDPP8** (as shown in the absorption spectra figure 2).

The IPCE values of the optimized devices based on **CSDPPs** are illustrated in figure 7b (**CSDPP5** and **CSDPP7**) and figure 8b (**CSDPP6** and **CSDPP8**). The IPCE response for four devices in the lower wavelength region corresponds to absorption spectra of $PC_{71}BM$ and is almost same. The device based on **CSDPP6**:$PC_{71}BM$ exhibit a broad and high IPCE values from 520 nm to 720 nm exceeding 47%. In comparison, the IPCE values of the device fabricated from **CSDPP8**:$PC_{71}BM$ are lower and also the response range is relatively narrower than that of the device based on **CSDPP**6:$PC_{71}BM$. The J_{sc} values estimated from integrating the IPCE spectra are 7.82 mA/cm^2 and 6.36 mA/cm^2 for **CSDPP6**:$PC_{71}BM$ and **CSDPP8**:$PC_{71}BM$, respectively, which is in good agreement with the experimentally observed J_{sc} values obtained from J-V characteristics under illumination. These IPCE spectra of the devices from **CSDPP6** and **CSDPP8** are consistent with the corresponding UV-Visible absorption spectra and confirm that **CSDPP6** having phenoxazine donor units can broaden the IPCE spectra and hence improve the PCE.

The electron and hole mobilities of the active layers were measured by space charge limited current (SCLC) method[32,58] using J-V characteristics of the electron only and hole only devices in dark (figure 9). The **CSDPP8**:$PC_{71}BM$ based device exhibits a hole and electron mobility of 6.44 x10^{-6} cm^2/Vs and 2.18 x10^{-4} cm^2/Vs, respectively. The device based on **CSDPP6**:$PC_{71}BM$ shows a high hole mobility of 9.56 x10^{-6} cm^2/Vs and almost same

electron mobility as for **CSDPP8**:$PC_{71}BM$ based device. The electron to hole mobility ratio of the devices based on **CSDPP5**:$PC_{71}BM$ and **CSDPP7**:$PC_{71}BM$ is 25 and 38, and that of **CSDPP6**:$PC_{71}BM$ and **CSDPP8**:$PC_{71}BM$ are 22 and 32 respectively. The more balanced charge transport of the device based on **CSDPP6**:$PC_{71}BM$ active layer is reflected from the higher PCE.

The low PCEs for the above devices based on the active layer processed with THF solvent are mainly due to the low values of J_{sc} and FF, although the V_{oc} is quite high. The series resistance (R_s) derived from the J-V characteristics of the devices, under illumination at voltage equivalent to V_{oc}, is very large (234 Ω cm^2 and 168 Ω cm^2 for **CSDPP8**:$PC_{71}BM$ and **CSDPP6**:$PC_{71}BM$, respectively). In general, R_s is mainly arising from bulk resistance of active layer, electron and hole transporting layers. Bulk resistance of the active layer can easily tunable via improving the film morphology using different treatments, i.e. thermal annealing,[59,60] solvent annealing[61,62] and solvent additives[63-65] that would enhance the charge carrier mobilities. The higher boiling point solvent additives are known to improve the morphology and charge carrier mobilities by reducing the molecular aggregation. Moreover, the relatively large exciton binding energy (0.3 eV) and short diffusion length (10-20 nm) of organic semiconductors warrants a large D/A interfacial area for efficient exciton dissociation and charge transport in BHJ OSCs. However, if the scale phase separated domains in BHJ layer is smaller than the coulomb capture radius, it will increase either germinate or bimolecular recombination probability. Therefore, an optimum nanomorphology and phase separation is required for efficient OSCs. Particularly, the choice of the solvent plays an important role and greatly influence the morphology of the active layer, since the morphology of the active layer depends upon the evaporation rate of the solvents. In an effort to improve the performance of the BHJ OSC based on **CSDPP6**:$PC_{71}BM$ and **CSDPP8**:$PC_{71}BM$ active layer, we employed solvent additive (DIO) method and optimized the concentration of DIO as 3% v, i.e. DIO (3v%) /THF solvent. The current–voltage characteristics of the resulting device is shown in figure 10a (**CSDPP6**:$PC_{71}BM$ (black color) and **CSDPP8**:$PC_{71}BM$ (red color)) and corresponding photovoltaic parameters are compiled in table 3. Remarkably, the PCE of the solar cell was improved from 3.06 % to 4.69 % and 2.43 % to 4.14 % for **CSDPP6**:$PC_{71}BM$ and **CSDPP8**:$PC_{71}BM$ based devices, respectively.

The superior performance of OSC based on **CSDPP6**:$PC_{71}BM$ processed with solvent additive is attributed to its improved J_{sc} (10.48 mA/cm^2) and FF (0.56) values. The improved J_{sc} value is ascribed to the enhanced IPCE response of the solar cell. As shown in figure 10b,

the devices with active layer processed with DIO/THF solvent exhibit a stronger and broader IPCE response compared to THF processed active layer. The J_{sc} depends upon the light harvesting capability of the active layer. As can be seen from the absorption spectra, (figure 6) the active layer cast from the DIO/THF showed higher absorption coefficient, particularly in the longer wavelength region, indicating that the active layer improved light harvesting efficiency, resulting high value of FF.

The photovoltaic performance of the organic BHJ solar cells is closely related with the nanomorphology of the active layer, we have investigated the film morphologies of **CSDPP6**:$PC_{71}BM$ (1:2) blend film cast from THF and DIO/THF solvents, from the atomic force microscopy (AFM), in tapping mode. Figure 11 shows AFM height images of the blend films processed with THF and DIO/THF. The blend film cast from THF solvent showed a relatively homogeneous and flat surface with a root mean squared (RMS) surface roughness of 0.62 nm and poor phase separation. However, the spin coated film from DIO/THF has slightly more aggregated domains and a phase separated surface with larger RMS roughness of 1.64 nm. Similar results for **CSDPP8**:$PC_{71}BM$ were observed with surface roughness of 0.54 nm and 1.46 nm for the film cast from THF and DIO/THF, respectively. The aggregated domains may be likely originated from the enhanced intermolecular interaction of SM (solvent medium), during the film formation.[66,67] A higher surface roughness is expected to increase the internal light scattering and enhance the light absorption,[68] consistent with the absorption spectra displayed in figure 6. The blend film with larger domain size suggests a good phase separation and well connected domains allow efficient charge generation and charge transfer within the active layer. The sum of all these effects enhances the J_{sc} and PCE for the device processed with DIO/THF solvent than that exhibited by device processed with THF only.

For the efficient OSCs, the mobility of electrons and hole in the BHJ active layer is also of great importance, as these should be balanced in order to achieve efficient charge transport and collection at the different electrodes. The mobility of holes and electrons in the **CSDPP6**:$PC_{71}BM$ active layer film cast from THF and DIO/THF were estimated from hole only device (ITO/PEDOT:PSS/**CSDPP6**:$PC_{71}BM$/Au) and electron only device (ITO/Al/**CSDPP6**:$PC_{71}BM$/Al), respectively, prepared from THF and DIO/THF processed films, by means of space charge limited current (SCLC) measurements.[69] The current – voltage characteristics of the hole only devices are shown in figure 12. The hole and electron mobilities were estimated by fitting the experimental data in the following equation.

$$J = \frac{9}{8}\varepsilon_o \varepsilon_r \mu \frac{V^2}{L^3}$$

Where ε_o and ε_r are the permittivity of free space and relative dielectric constant of active layer, respectively, μ is the charge carrier mobility and L is the thickness of the active layer. The hole mobilities for the blend films processed with and without solvent additive were 3.56×10^{-5} cm^2/V, 9.56×10^{-6} cm^2/V for **CSDPP6**:$PC_{71}BM$ and 2.63×10^{-5}, 6.44×10^{-6} for **CSDPP8**:$PC_{71}BM$ respectively. The hole mobilities for the blend films processed with additive are higher than those for the films cast without additive. The improved hole mobility may be attributed to the well defined phase separation as revealed from the AFM results. On the contrary, the electron mobility was slightly increased from 2.18×10^{-4} cm^2/Vs (THF cast) to 2.23×10^{-4} cm^2/Vs (DIO/THF cast). For the efficient BHJ OSCs, the electron/hole mobilities ratio should be as low as possible, so that the charge transport should be balanced (unity, for an ideal organic solar cell). The ratio of electron and hole mobilities for the blends (**CSDPP6**:$PC_{71}BM$ and **CSDPP8**:$PC_{71}BM$) cast from solution with and without additive were 6.2, 22 and 8.9, 32 respectively, indicating a more balanced charge transport in the device blends processed with additive. The smaller value of mobility ratio indicates a more balanced charge transport that reduces the space-charge effect and results in an improvement in the Jsc and overall PCE. If the charge transport in the device is unbalanced (blend cast from THF, where the mobility ratio is high), hole accumulation occurs in the device and the photocurrent is space-charge limited.[70]

4. Conclusions

Four solution processed D-A-D small molecules based on DPP as central acceptor core and different terminals, i.e. carbazole (**CSDPP7**, **CSDPP8)** and phenoxazine (**CSDPP5**, **CSDPP6)** donor units were synthesized and their optical and electrochemical properties investigated. The LUMO energy level of these small molecules is almost same as that of DPP acceptor, but exhibit different HOMO levels due to the presence of different donor units. The BHJ OSCs **CSDPP5**:$PC_{71}BM$ (1:2w/w), **CSDPP6**:$PC_{71}BM$ (1:2 w/w) **CSDPP7**:$PC_{71}BM$ (1:2 w/w) and **CSDPP8**:$PC_{71}BM$ (1:2 w/w) processed with THF showed overall PCE of about 2.97 %, 3.06 %, 2.42 % and 2.43 %, respectively. The incorporation of 3 % v DIO as solvent additive enhanced the PCE of **CSDPP6**:$PC_{71}BM$ and **CSDPP8**:$PC_{71}BM$ up to 4.69 % and 4.14 %, attributed to the better phase separation nanomorphology of the active layer and enhanced charge transportation in the active layer. From above results, we conclude that the terminal donor significantly affect the PCEs of the BHJ OSCs.

ASSOCIATED CONTENT

*Supporting Information

Structures of optimized geometries, molecular orbitals, Percentage contributions of the orbital density of the individual groups, calculated excitation energies, calculated HOMOs and LUMOs energy levels, optimized geometry parameters of **CSDPP5-CSDPP8** calculated at B3LYP/6-311 G(d,p) level theory.

Acknowledgements

Ch. P.K. thanks UGC, New Delhi for a senior research fellowship.

References

1. Y. J, Cheng, S. H.Yang and C. S. Hsu, *Chem. Rev*., 2009, **109,** 5868-5923.
2. G. Li, R. Zhu, and Y. Yang, *Nat. Photonics*, 2012, **6**, 153-161.
3. K. Li, Z. Li, K. Feng, X. Xu, L. Wang and Q. Peng, *J. Am. Chem. Soc.,* 2013, **135**, 13549-13557.
4. H. L. Yip and A. K. Y. Jen, *Energy Environ. Sci.,* 2012, **5**, 5994-6011.
5. J. Chen and Y. Cao, *Acc. Chem. Res.,* 2009, **42,** 1709-1718.
6. L. Dou, J. You, Z. Hong, Z. Xu, G. Li, R. A. Street and Y. Yang, *Adv. Mater.,* 2013, **25**, 6642-6671.
7. Z. He, C. Zhong, S. Su, M. Xu, H. Wu and Y. Cao, *Nat. Photonics*, 2012, **6**, 591–595.
8. S. H. Liao, H. J. Jhuo, Y. S. Cheng and S. A. Chen, *Adv. Mater.,* 2013, **25**, 4766-4771.
9. A. M. Abakumov, A. a. Tsirlin, I. Bakaimi, G. V. Tendel and A. Lappas, *Chem., Mater.* 2014, **26**, 3306-3315.
10. X. Guo, M. Zhang, W. Ma, L. Ye, S. Zhang, S. Liu, H. Ade, F. Huang and J. Hou, *Adv. Mater*., 2014, **26**, 4043–4049.
11. W. Zhang, Y. Wu, Q. Bao, F. Gao and J. Fang, *Adv.Energy Mater.,* 2014, DOI: 10.1002/aenm.201400359.

12. Y. Liu, J. Zhao, Z. Li, C. Mu, W. Ma, H. Hu, K. Jiang, H. Lin, H. Ade, and H. Yan *Nat. commun. ,* 2014, **5**, 5293-5301.
13. B. Kan, M. Li, Q. Zhang, F. Liu, X. Wan, Y. Wang, W. Ni, G. Long, X. Yang, H. Feng, Y. Zuo, M. Zhang, F. Huang, Y. Cao, T. P. Russell, and Y. Chen, *J. Am. Chem. Soc.,* 2015, **137**, 3886-3893.
14. A. R. B. M. Yusoff, D. Kim, H. P. Kim, F. K. Shneider, W. J. da Silva, and J. Jang *Energy Environ. Sci.,* 2015, **8**, 303-316.
15. C.-C. Chen, W.-H. Chang, K. Yoshimura, K. Ohya, J. You, J. Gao, Z. Hong and Y. Yang, *Adv. Mater.,* 2014, **26**, 5670–5677.
16. A. A. Virkar, S. Mannsfeld, Z. N. Bao and N. Stingelin, *Adv. Mater.,* 2010, **22,** 3857-3875.
17. Z. He, H. Wu and Y. Cao, *Adv. Mater.,* 2014, 26, 1006-1024.
18. X. Gao and Y. Hu, *J. Mater. Chem. C*, 2014, **2**, 3099-3117.
19. A. Mishra and P. Bäuerle, *Angew. Chem., Int. Ed.,* 2012, **51**, 2020-2067.
20. Y. Lin, Y. Li and X. Zhan, *Chem. Soc. Rev.,* 2012, **41**, 4245-4272.
21. Y. Sun, G. C. Welch, W. L. Leong, C. J. Takacs, G. C. Bazan and A. J. Heeger, *Nature Mater.,* 2012, **11**, 44-48.
22. J. E. Coughlin, Z. B. Henson, G. C. Welch and G. C. Bazan, *Acc. Chem. Res.*, 2014, **47,** 257-270.
23. J. Zhou, X. Wan, Y. Liu, Y. Zuo, Z. Li, G. He, G. Long, W. Ni, C. Li, X. Su and Y. Chen, *J. Am. Chem. Soc.*, 2012, **134**, 16345–16351.
24. A. K. K. Kyaw, D. H. Wang, D. Wynands, J. Zhang, T. Q. Nguyen, G. C. Bazan and A. J. Heeger, *Nano Lett.,* 2013, **13**, 3796-3801.
25. J. Zhou, Y. Zuo, X. Wan, G. Long, Q. Zhang, W. Ni. Y. Li, Z. Li, G. Su, C. Li, B. Kan, M. Li and Y. Chen, *J. Am. Chem. Soc.*, 2013, **135**, 8484-8487.
26. Y. Chen, X. Wan and G. Long, *Acc. Chem. Res.*, 2013, **46**, 2645-2655.
27. Y. Liu, C. Chen, Z. Hong, J. Gao, Y. Yang, H. Zhou, L. Dou, G. Li and Y. Yang, *Sci. Rep.*, 2013, **3,** 3356/1-8.
28. B. Kan, Q. Zhang, M. Li, X. Wan, W. Ni, G. Long, Y. Wang, X. Yang, H. Feng and Y. Chen, *J. Am. Chem. Soc.*, 2014, **136**, 15529–15532.
29. Heliatek consolidates its technology leadership by establishing a new world record for organic solar technology with a cell efficiency of 12%. Available at http://www.heliatek.com/en/press/press-releases/details/heliatek-consolidates-its-

technology-leadership-by-establishing-a-new-world-record-for-organic-solar-technology-with-a-cell-effi (2013) accessed July 22, 2014.

30. B. Tamayo, M. Tantiwiwat, B. Walker and T. Q, Nguyen, *J. Phys. Chem. C,* 2008, **112,** 15543-15552.
31. A. B. Tamayo, X. D. Dang, B. Walker, J. Seo, T. Kent and T. Q. Nguyen, *Appl. Phys. Lett.*, 2009, **94**, 103301-103302.
32. B. Walker, A. B. Tamayo, X. D. Dang, P. Zalar, J. H. Seo, A. Garcia, M. Tantiwiwat and T. Q. Nguyen, *Adv. Funct. Mater.*, 2009, **19**, 3063-3069.
33. J. Liu, B. Walker, A. Tamayo, Y. Zhang and T. Q. Nguyen, *Adv. Funct. Mater.*, 2013, **23,** 47-56.
34. S. Qu and H. Tian, *Chem. Commun.*, 2012, **48**, 3039-3051.
35. O. P. Lee, A. T. Yiu, P. M. Beaujuge, C. H. Woo, T. W. Holcombe, J. E. Millstone, J. D. Douglas, M. S. Chen and J. M. Fréchet, *Adv. Mater.*, 2011, **23**, 5359-5363.
36. C. Kim, J. Liu, J. Lin, A. B. Tamayo, B. Walker, G. Wu and T. Q. Nguyen, *Chem. Mater.*, 2012, **24**, 1699-1709.
37. B. Zhao, K. Sun, F. Xue and J. Ouyang, *Org. Electron.*, 2012, **13**, 2516-2524.
38. M. Chen, W. Fu, M. Shi, X. Hu, J. Pan, J. Ling, H. Li and H. Chen, *J. Mater. Chem. A,* 2013, **1,** 105-111.
39. J. Liu, Y. Sun, P. Moonsin, M. Kuik, C. M. Proctor, J. Lin, B. B. Hsu, V. Promarak, A. J. Heeger and T. Q. Nguyen, *Adv. Mater.*, 2013, **25**, 5898–5903.
40. W. Li, W. S. C. Roelofs, M. M. Wienk and R. A. J. Janssen, *J. Am. Chem. Soc.,* 2012, **134,** 13787-13795.
41. H. Bronstein, Z. Chen, R. S. Ashraf, W. Zhang, J. Du, J. R. Durrant, P. S.Tuladhar, K. Song, S. E. Watkins, Y. Geerts, M. M. Weink, R. A. J. Janssen, T. Anthopoulos, H. Sirringhaus, M. Heeney and I. McCulloch, *J. Am. Chem. Soc.*, 2011, **133**, 3272-3275.
42. L. Dou, J. Gao, E. Richard, J. You, C. C. Chen, K. C. Cha, Y. He, G. Li and Y. Yang, *J. Am. Chem. Soc.*, 2012, **134**, 10071-10079.
43. H. Qin, L. Li, F. Guo, S. Su, J. Peng, Y. Cao and X. Peng, *Energy Environ. Sci.*, 2014, **7**, 1397–1401.
44. M. Cheng, X. Yang, C. Chen, Q. Tan and L. Sun, *J. Mater. Chem. A*, 2014, **2**, 10465–10469.
45. G. D. Sharma, M. Anil Reddy, K. Ganesh, S. P. Singh and M. Chandrasekharam, *RSC Adv.*, 2014, **4**, 732-42.

46. M. Chandrasekharam, M. Anil Reddy, K. Ganesh, G. D. Sharma, S. P. Singh and J. Laxmikanth Rao, *Organic Electronics*, 2014, **15**, 2116–2125.
47. CH. Pavan Kumar, K. Ganesh, T. Suresh, Abhishek Sharma, K. Bhanuprakash, G. D. Sharma and M. Chandrasekharam RSC Adv., 2015, **5**, 93579–93590
48. A. Iqbal, M. Jost, R. Kirchmayr, J. Pfenninger, A. Rochat and O. Wallquist, *Bull. Soc. Chim. Belg.,* 1988, **97**, 615–643.
49. A. C. Rochat, L. Cassar and A. Iqbal, *European Patent* 0094911, 1983.
50. N. Avcibasi, M. Smet, B. Metten, W. Dehaen, F. C. De Schryver, G. Bultynck, G. Callewaert, H. De Smedt, L. Missiaen and N. Boens, *Int. J. Photoenergy*, 2004, **6**, 159–167.
51. M. J. Frisch, G. W. Trucks, H. B. Schlegel, G. E. Scuseria, M. A. Robb, J. R. Cheeseman, G. Scalmani, V. Barone, B. Mennucci, and G. A. Petersson, Gaussian 09, Revision B.01, Gaussian, Inc., Wallingford, CT, 2010.
52. A. D. Becke, *J. Chem. Phys.*, 1993, **98**, 5648-5652.
53. A. D. Becke, *J. Chem. Phys.,* 1996, **104**, 1040.
54. G. A. Petersson, A. Bennett, T. G. Tensfeldt, M. A. Al-Laham, W. A. Shirley, and J. Mantzaris, *J. Chem. Phys.*, 1988, **89,** 2193-2198.
55. M. Cossi, V. Barone, R. Cammi, and J. Tomasi, *Chem. Phys. Lett,* 1996, **255**, 327-335.
56. N. M. O'Boyle, A. L. Tenderholt, and K. M. Langner, *J. Comput. Chem.,* 2008, **29,** 839-845.
57. K. Chandrasekhar, L. R. Naik, H. M. Suresh Kumar and N.N. Math, Indian J Pure & Appl Phys., 2006, 44, 292-299.
58. M. A. Khan, W. Xu, H. Khizarul, Y. Bai, X. Y. Jiang, Z. L. Zhang, W. Q. Zhu, Z. L. Zhang and W. Q. Zhu, *J. Appl. Phys.,* 2008, **103,** 014509/1-4.
59. W. Ma, C. Yang, X. Gong, K. Lee and A. J. Heeger, *Adv. Funct. Mater.,* 2005, **15**, 1617−1622.
60. J. A. Mikroyannidis, A. N. Kabanakis, S. S. Sharma and G. D. Sharma, *Adv. Funct. Mater.*, 2011, **21**, 746-755.
61. G. Li, V. Shrotriya, J. S. Huang, Y. Yao, T. Moriarty, K. Emery and Y. Yang, *Nat. Mater.,* 2005, **4**, 864−868.
62. Y. Zhao, Z. Xie, Y. Qu, Y. Geng and L. Wang, *Appl. Phys. Lett.*, 2007, **90**, 043504/1−3.

63. A. Tamayo, T. Kent, M. Tantitiwat, M. A. Dante, J. Rogers and T. Q. Nguyen, *Energy Environ. Sci.*, 2009, **2,** 1180−1186.
64. C. Min, J. Li, G. Veronis, J. Y. Lee, S. Fan, and P. Peumans, *Appl. Phys. Lett.*, 2010, **97**, 133302/1−3.
65. B. Walker, C. Kim and T. Q. Nguyen, *Chem. Mater.*, 2010, **23,** 470−482.
66. Q. Shi, P. Cheng, Y. Li and X. Zhan, *Adv. Energy Mater.*, 2012, **2**, 63-67.
67. A. K. K. Kyaw, D. H. Wang, C. Luo, Y. Cao, T. Q. Nguyen, G. C. Bazan and A. J. Heerger, *Adv. Energy Mater.*, 2014, **4**, DOI: 10.1002/aenm.201301469.
68. J. D. Zimmermen, X. Xiao, C. K. Renshaw, S. Wang, V. V. Diev, M. E. Thompson and S. R. Forrest, *Nano. Lett.*, 2012, **12**, 4366-4371.
69. G. G. Malliaras, J. R. Salem, P. J. Brock and C. Scott, *Phys. Rev. B: Condens. Matter Mater. Phys.,* 1998, **58**, 13411–13414.
70. A. J. Moule and K. Meerholz, *Adv. Mater.*, 2008, **20**, 240-245.

Table 1 Photophysical and electrochemical data for the **CSDPP5**, **CSDPP6**, **CSDPP7** and **CSDPP8**

Dye	λ_{max}[a] (ε X10^{-4} $M^{-1}cm^{-1}$) [nm]	E_{ox} (V)[b]/E_{HOMO} (eV)	$E_{0\text{-}0}$ (eV)[c]	E_g(opt) (eV)[d]	E_{LUMO} (V)[d]/ E_{LUMO} (eV)
CSDPP5	647 (6.3899)	0.546 (-5.24)	1.846	1.65	-1.30 (-3.39)
CSDPP6	647(6.5494)	0.534 (-5.23)	1.845	1.66	-1.31 (-3.39)
CSDPP7	623 (6.9098)	0.603 (-5.30)	1.937	1.77	-1.33 (-3.36)
CSDPP8	623(6.5046)	0.623 (-5.32)	1.933	1.78	-1.31 (-3.39)

[a]Absorption spectra were recorded in THF solutions at 298K
[b]The oxidation potentials (Eox *vs* NHE) of these dyes are corresponding to the HOMO levels.
[c]$E_{0\text{-}0}$, was derived from the intersection of the absorption and emission spectra
[d] optical bandgap estimated from the onset absorption edge of absorption spectra in thin film
[f] $E_{LUMO} = Eox - E_{0\text{-}0}$

Table 2. Calculated properties of the **CSDPP5-CSDPP8** using B3LYP/6-311G(d,p). Specifically HOMO and LUMO energies (eV), HOMO–LUMO gap (eV), *HLG*, with corresponding oscillator strengths, *f*, the wavelengths of the first excitation and excitations with the largest oscillator strengths, the main contributions to the first excited state, and the dipole moment (D), μ.

CSDPPs	λ_{max} [a] (nm)	λ_{max}(nm)	HOMO	LUMO	HLG	*f*	Main Contribution	μ (D)
CSDPP5	647	615	-5.18	-2.88	2.30	1.216	H → L (99%)	0.89
CSDPP6	647	624	-5.16	-2.91	2.25	1.214	H → L (99%)	1.47
CSDPP7	623	606	-5.06	-2.75	2.31	1.505	H → L (99%)	0.29
CSDPP8	623	615	-5.04	-2.77	2.27	1.489	H → L (99%)	0.21

[a] absorption values obtained from experimental data.

Table 3. Photovoltaic parameters of the BHJ organic solar cells, using **CSDPP5**, **CSDPP6** and **CSPPP7** and **CSDPP8** as donor and $PC_{71}BM$ as acceptor, the optimized donor to acceptor is 1:2 in each device

Blend	J_{sc} (mA/cm^2)	V_{oc} (V)	FF	PCE (%)	μ_h (cm^2/Vs)	μ_e/μ_h
CSDPP5:$PC_{71}BM$[a]	7.88	0.84	0.47	2.97	9.48x10^{-6}	25
CSDPP6:$PC_{71}BM$[a]	7.92	0.84	0.46	3.06	9.56 x10^{-6}	22
CSDPP7:$PC_{71}BM$[a]	6.34	0.91	0.42	2.42	6.38x10-6	38
CSDPP8:$PC_{71}BM$[a]	6.42	0.90	0.42	2.43	6.44 x10^{-6}	32
CSDPP6:$PC_{71}BM$[b]	10.48	0.80	0.56	4.69	3.56 x10^{-5}	6.2
CSDPP8:$PC_{71}BM$[b]	8.92	0.86	0.52	4.14	2.63x10^{-5}	8.9

[a]processed with THF
[b]processed with DIO/THF

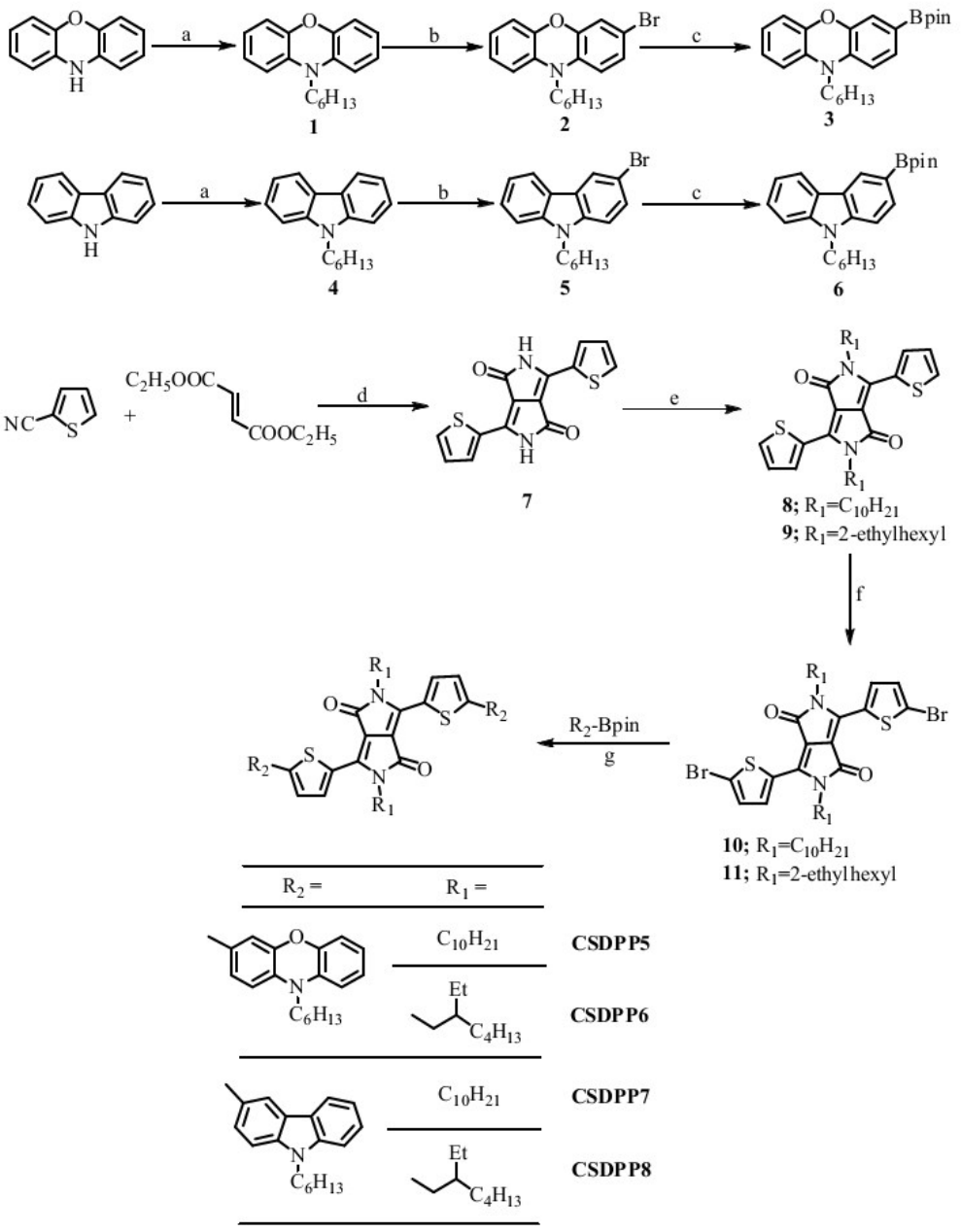

Reagents and conditions: a) 1.2 eq. bromohexane, NaH, DMF, RT, 18 h; b) 1.1 eq. N -bromosuccinimide, $CHCl_3$, RT, 6 h; c) 1.1 eq. bis(pinacolato)diboron (B_2pin_2), 0.05 eq. $PdCl_2$ (dppf), 3 eq. KOAC, dry DME, reflux, 18 h; d) 0.5 eq. di -n-ethylsuccinate, *tert* -BuOK, *tert*-amyl alcohol 120°C, under Ar, 24 h; e) 2.5 eq R1-X, K_2CO_3, DMF, 130 °C, under Ar, 24 h; f) 2.05 eq. N-bromosuccinimide, $CHCl_3$, dark, under Ar, 12h; g) $Pd(PPh_3)_4$, 2 M Na_2CO_3, DME, 90°C, under Ar, 18 h

Scheme 1 Synthetic route of **CSDPP5**, **CSDPP6**, **CSDDP7** and **CSDPP8**

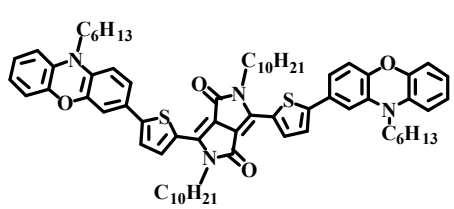

CSDPP5

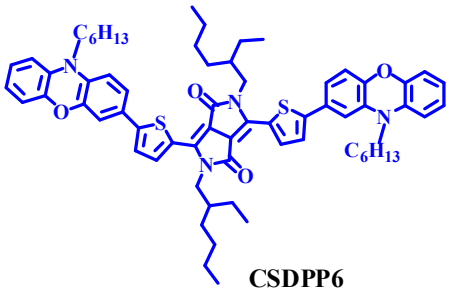

CSDPP6

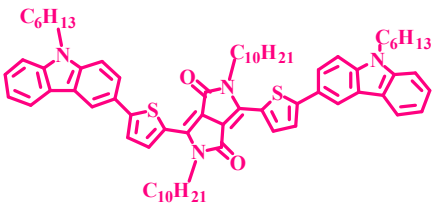

CSDPP7

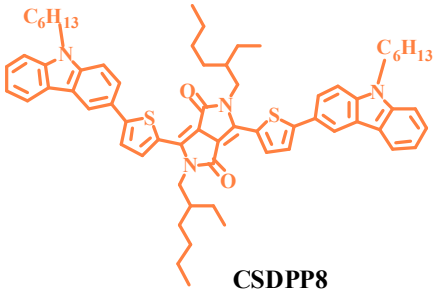

CSDPP8

Figure 1. Structures of **CSDPP5-CSDPP8**

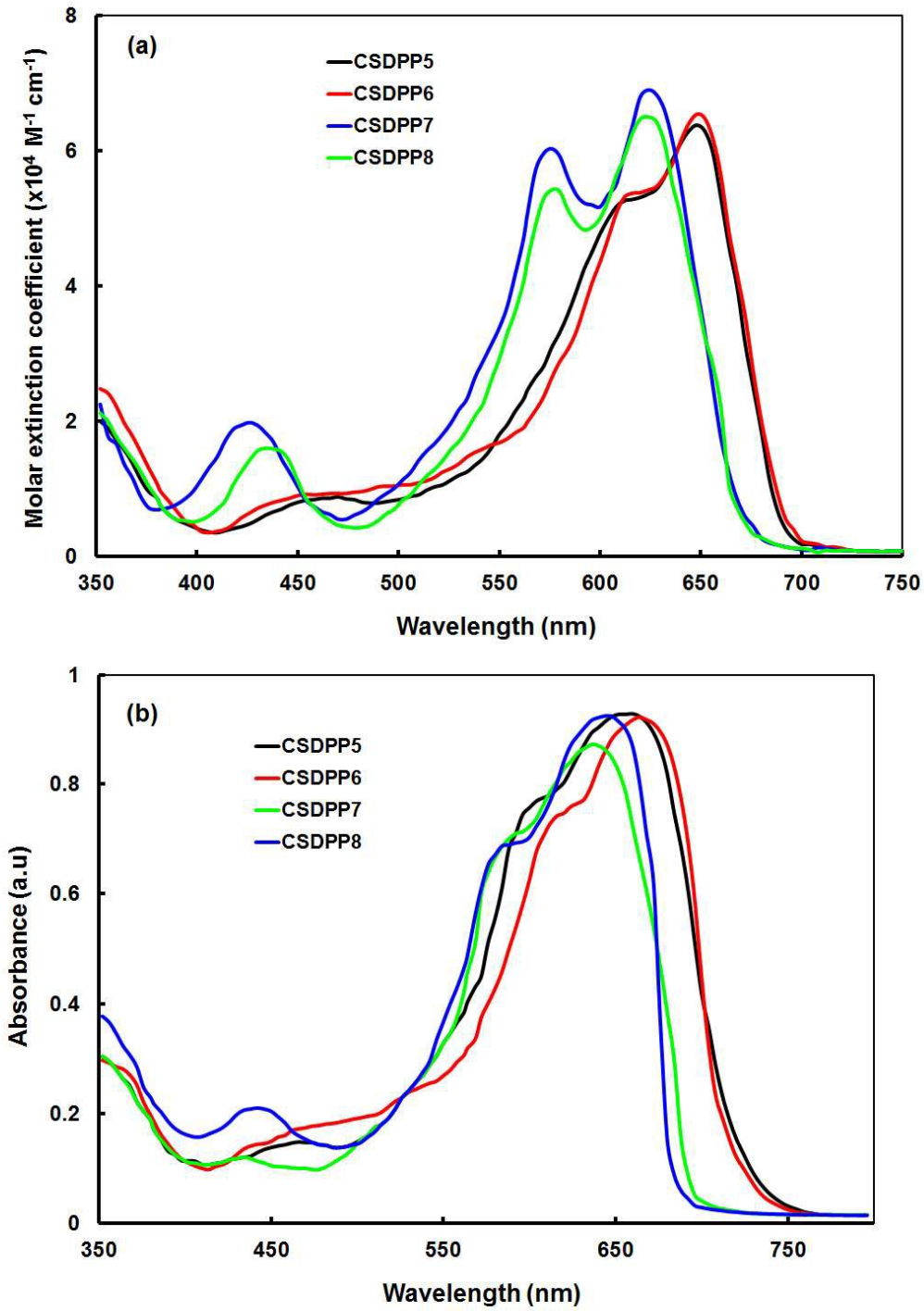

Figure 2. Optical absorption spectra of **CSDPP5**, **CSDPP6**, **CSDPP7** and **CSDPP8** in (a) dilute THF solution and (b) thin film cast from THF solvent

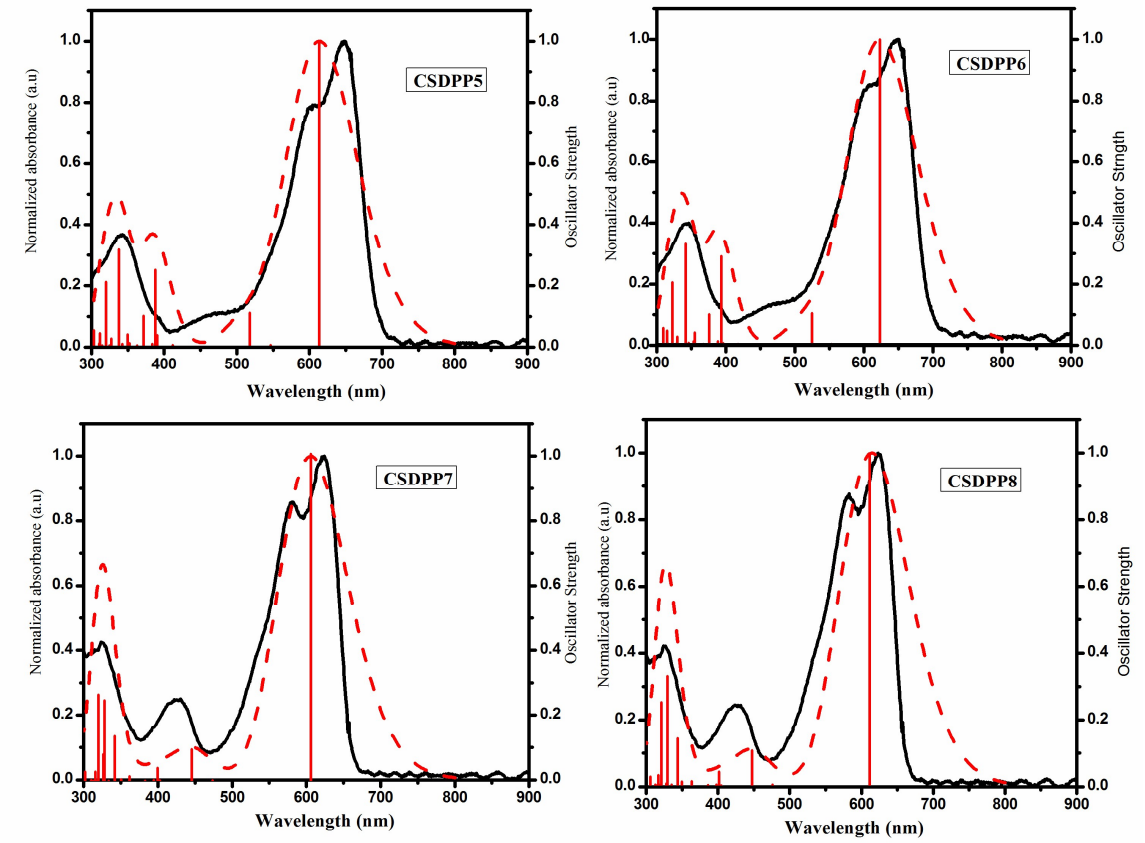

Figure 3. Comparison between experimental (black lines) and calculated (red lines) UV-Vis absorption spectra of the **CSDPP** dyes in THF solution. Red vertical lines represent the calculated singlet excitation energies in GaussSum 2.2.5.

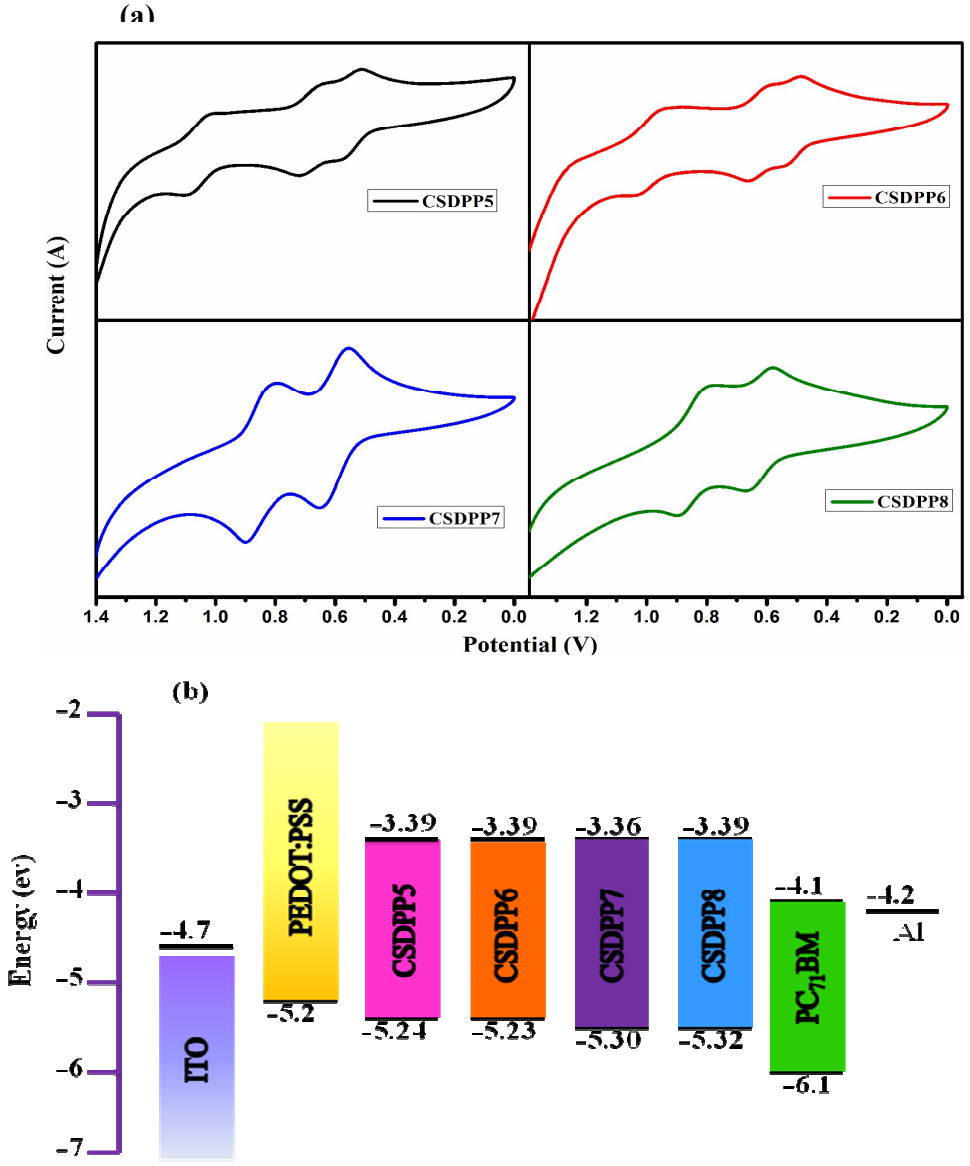

Figure 4. (a) Cyclic voltammograms of **CSDPP5**, **CSDPP6, CSDPP7** and **CSDPP8** in DCM;scan rate 100 mV s^{-1}; supporting electrolyte: tetrabutylammonium hexafluorophosphate (NBu_4PF_6). (b) Energy levels of different components in a photovoltaic device.

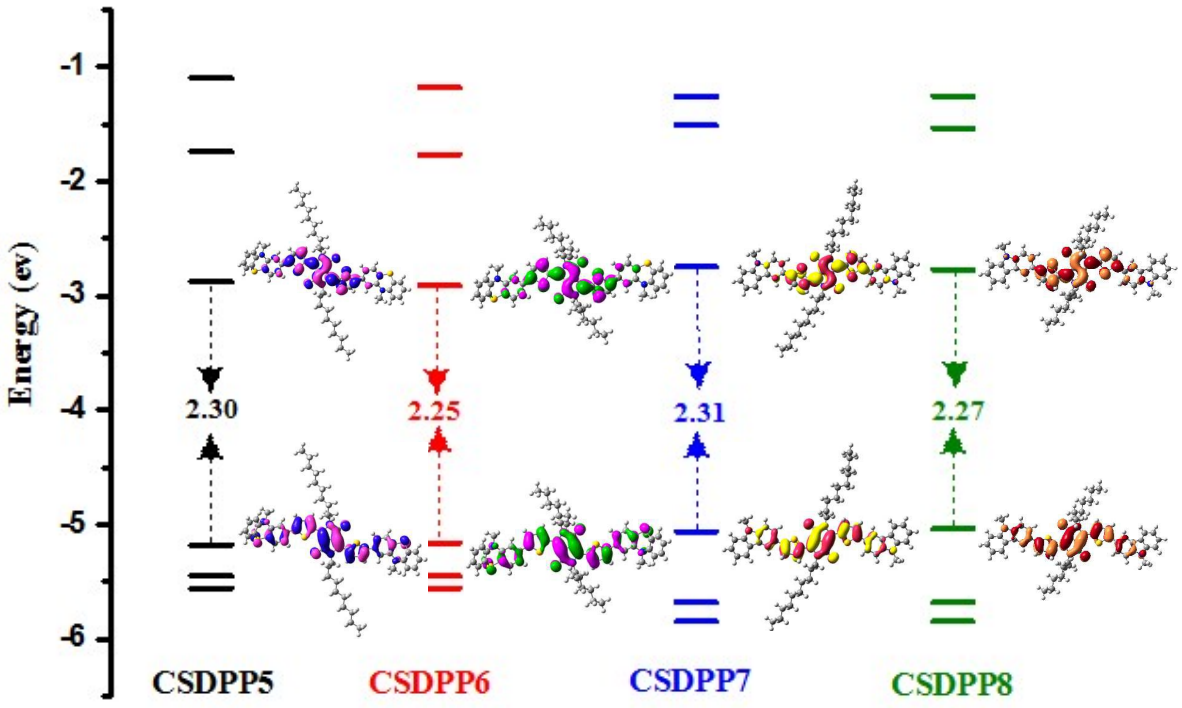

Figure 5. Calculated HOMO–LUMO gaps at B3LYP/6-311g(d, p) level of theory and respective HOMO and LUMO orbital pictures at B3LYP/6-311g(d, p)level of **CSDPPs** in THF solvent.

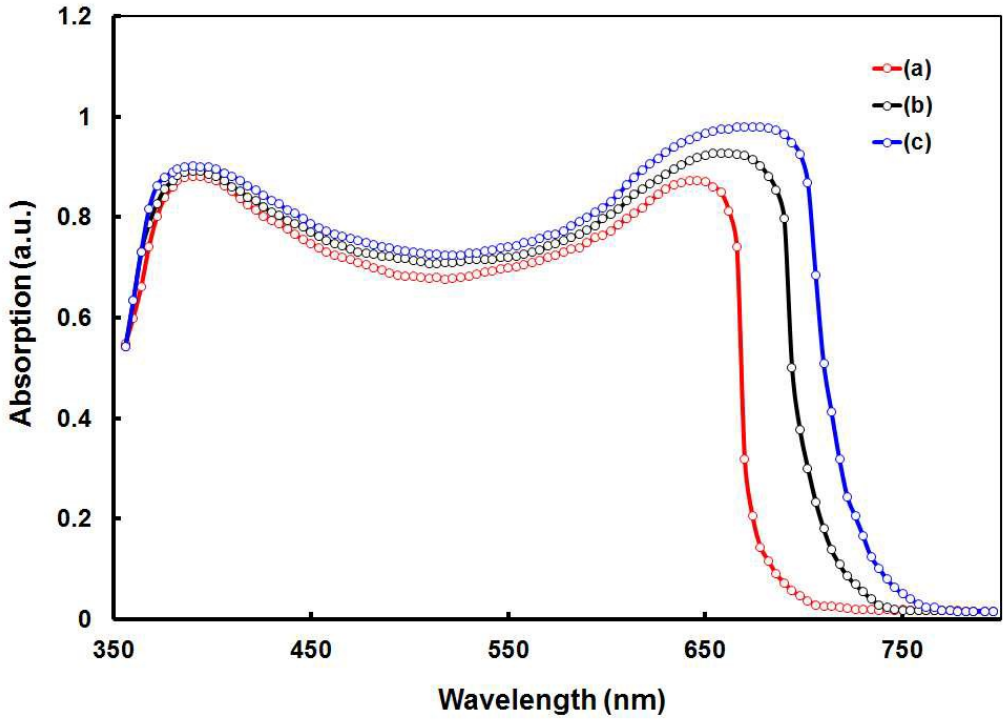

Figure 6. Absorption spectra of (a) **CSDPP8**:$PC_{71}BM$ (THF cast), (b) **CSDPP6**:$PC_{71}BM$ (THF cast), and (c) **CSDPP6**:$PC_{71}BM$ (DIO/THF cast) active layers

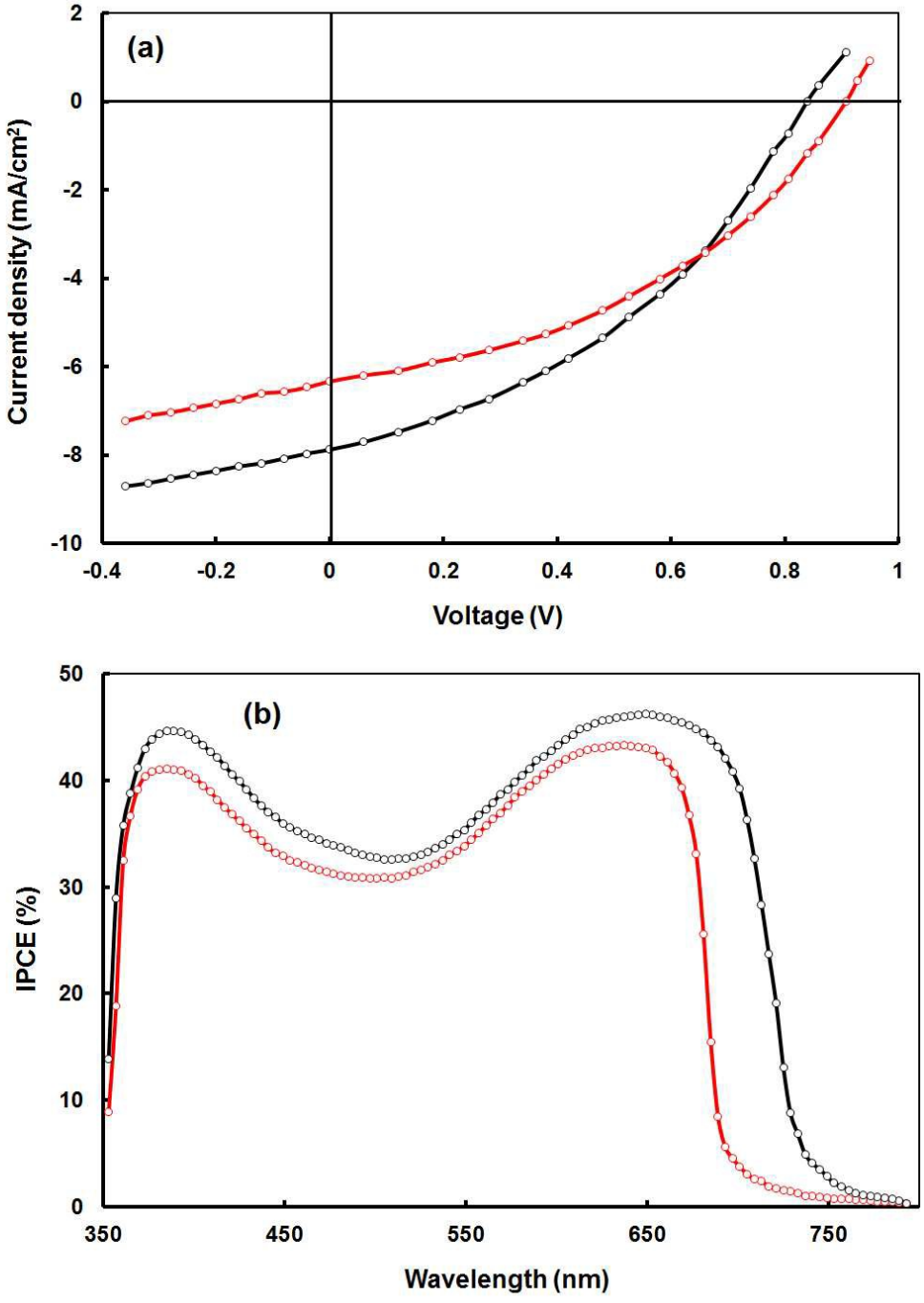

Figure 7 (a) Current –voltage (J-V) characteristics and (b) IPCE spectra of the BHJ solar cells based on **CSDPP5**:$PC_{71}BM$ (THF cast) (black color), **CSDPP7**:$PC_{71}BM$ (THF cast) (red color)

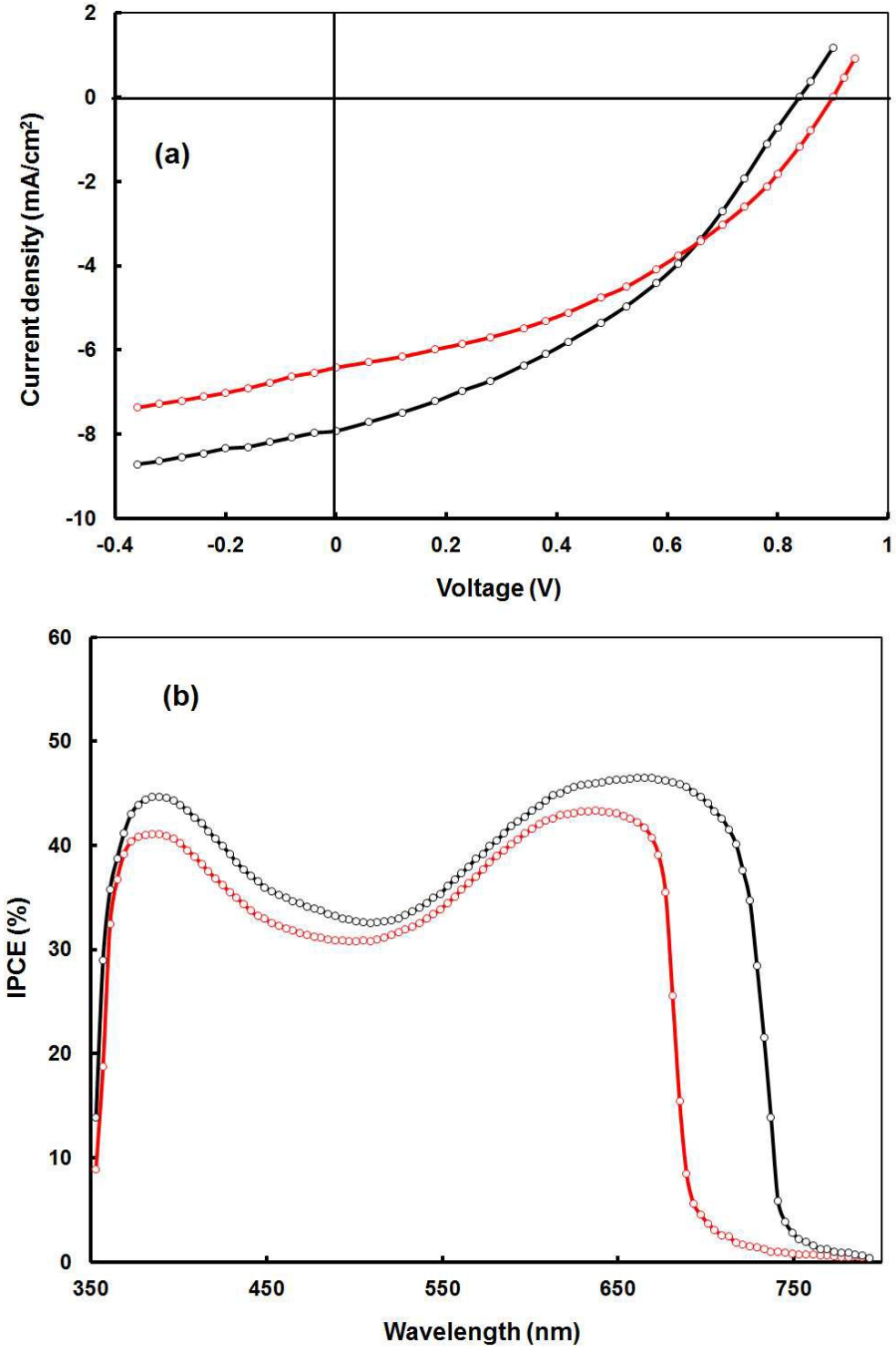

Figure 8 (a) Current –Voltage (J-V) characteristics and (b) IPCE spectra of the BHJ solar cells based on **CSDPP6**:$PC_{71}BM$ (THF cast) (black color) and **CSDPP8**:$PC_{71}BM$ (THF cast) (red color)

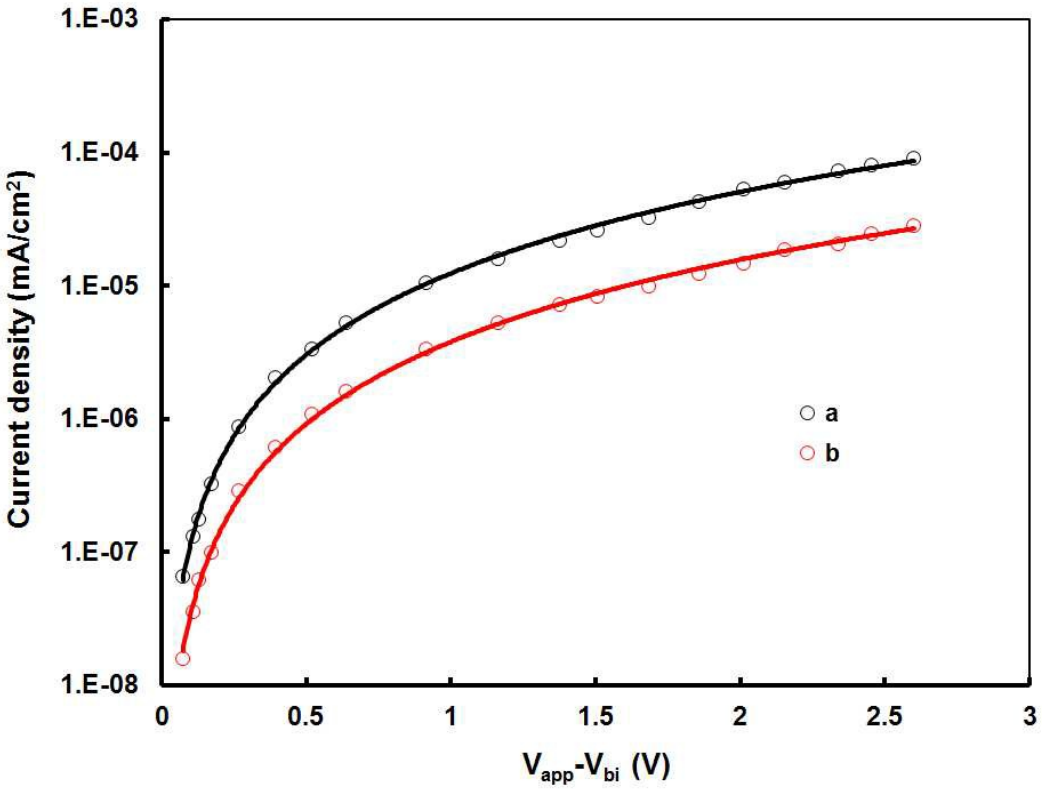

Figure 9. Current-Voltage (J−V) characteristics in dark for hole-only based on (a) **CSDPP6**:$PC_{71}BM$ (THF cast) active layer (black color) and (b) **CSDPP8**:$PC_{71}BM$ (THF cast) (red color).

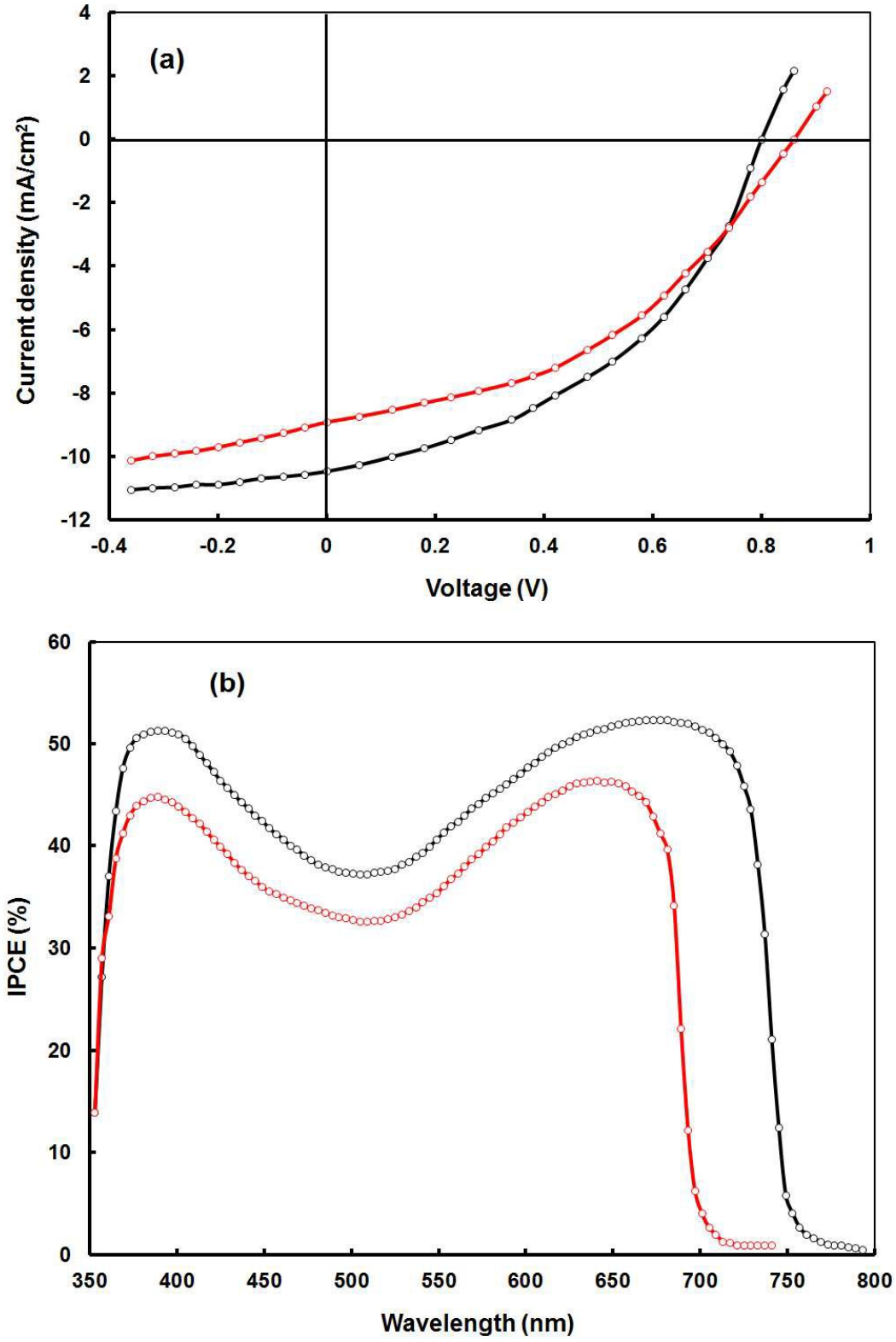

Figure 10 (a) Current –Voltage (J-V) characteristics and (b) IPCE spectra of the BHJ solar cells based on **CSDPP6**:$PC_{71}BM$ (DIO/THF cast) (black color) and **CSDPP8**:$PC_{71}BM$ (DIO/THF cast) (red color).

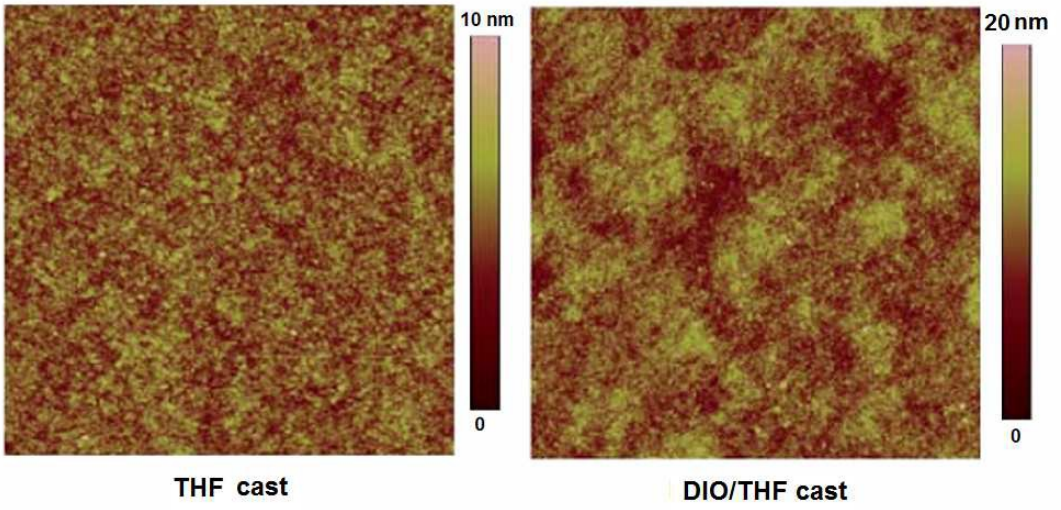

Figure 11. AFM height images of **CSDPP6**:$PC_{71}BM$ (1:2) films cast from THF and DIO/THF, scan sizes are 3μm x 3μm.

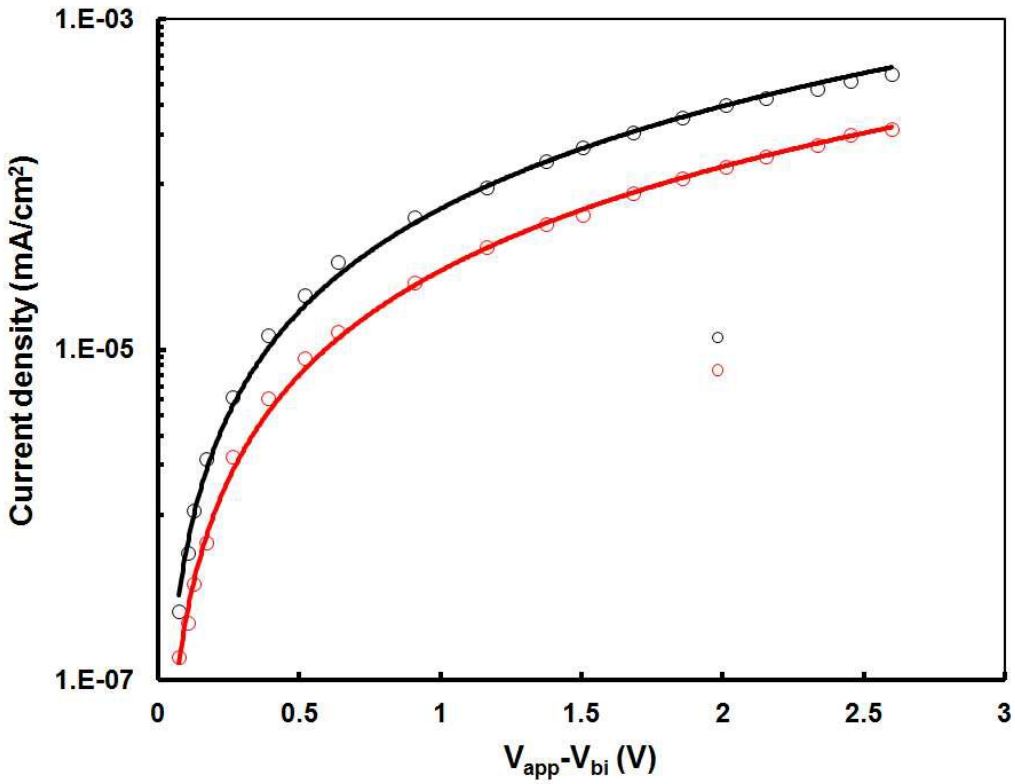

Figure 12. Current-Voltage (J−V) characteristics in dark for hole-only based on (a) **CSDPP6**:$PC_{71}BM$ (DIO/THF cast) active layer (black color) and (b) **CSDPP8**:$PC_{71}BM$ (DIO/THF cast) (red color)

TOC